Roles of Cell Surface Proteins During Cytokinesis

by

Ezgi Memiş

A Thesis Submitted to the
Graduate School of Sciences and Engineering
in Partial Fulfillment of the Requirements for
the Degree of

Master of Science

in

Molecular Biology and Genetics

January 6, 2021

Roles of Cell Surface Proteins During Cytokinesis

Koç University

Graduate School of Sciences and Engineering

This is to certify that I have examined this copy of a master's thesis by

Ezgi Memiş

and have found that it is complete and satisfactory in all respects,
and that any and all revisions required by the final
examining committee have been made.

Committee Members:

_____

Assoc. Prof. Nurhan Özlü (Advisor, Koç University)

_____

Prof. Ulrike Eggert (King's College London)

_____

Assist. Prof. Ayşe Koca Çaydaşı (Koç University)

Date: _____

This thesis is dedicated to my beloved family Sakine, Hakan, and Işıl for their unconditional love, support, and encouragement.

ABSTRACT

Identification of the Roles of Cell Surface Proteins During Cytokinesis

Ezgi Memiş

Master of Science in Molecular Biology and Genetics

January 6, 2021

Cell division requires many sequential and coordinated actions of chromosomes, cell cycle machinery, cytoskeleton, and cellular membranes. These events have been extensively studied in many cell biology laboratories. Among those, how cell surface components and intracellular cell cycle machinery communicate, especially during cytokinesis, is much understudied. In this project, we aim to determine the roles of cell surface proteins during cytokinesis. Previous studies in the Eggert lab have shown that Glypicans 3 and 5 might have a role in cytokinesis since silencing their expression causes multinuclear cells. Glypicans are members of heparan sulphate proteoglycans that are highly conserved among eukaryotes. They are covalently attached to the plasma membrane via GPI anchors where they entirely face the extracellular matrix. In this thesis, I determined cellular localization of Glypican 3 and 5 during cell division and characterized their cell division phenotype. We performed a mass spectrometry-based proximity interactome analyses of Glypicans 3 and 5 at interphase and dividing cells. Our study revealed that Glypican 5 might have important roles in cortical actin stability and midbody abscission. In addition, we identified several proteins as Glypican 3 and 5 interactors that might give insights about the molecular mechanisms underlying their role in cytokinesis.

ÖZETÇE

Hücre Yüzeyi Proteinlerinin Sitokinezdeki Rollerinin Belirlenmesi

Ezgi Memiş

Moleküler Biyoloji ve Genetik, Yüksek Lisans

6 Ocak 2021

Hücre bölünmesi; kromozomların, hücre bölünmesiyle ilişkilendirilmiş çeşitli proteinlerin, hücre iskeletinin ve hücre zarının koordineli çalışmaları ile gerçekleşen bir süreçtir. Bu olgular pek çok hücre biyolojisi laboratuvarında etraflıca araştırılmaktadır. Ancak hücre yüzeyi bileşenlerinin ve hücre içi bölünme mekanizmasının özellikle sitokinezde birbiriyle nasıl iletişim kurduklarını inceleyen çalışmaların sayısı oldukça azdır. Bu projede, hücre yüzeyi proteinlerinin hücre bölünmesindeki rollerini araştırmayı amaçladık. Eggert Laboratuvarında daha önceden yapılmış çalışmalar, Glypican 3 ve 5 proteinlerinin sitokinezde rol alıyor olabileceklerini ortaya çıkarmıştı. Glypicanlar ökaryotlar arasında evrimsel olarak hayli korunmuş olan heparan sülfat proteoglikanlarındandır. Glypicanlar sadece bir GPI modifikasyonuyla plazma membranına kovalent olarak bağlanmış olup, kendileri tamamen hücre dışı matrise bakacak şekilde konumlanmışlardır. Bu tezde, Glypican 3 ve 5 in hücre bölünmesi sırasındaki lokalizasyonlarını belirledim ve bölünme fenotiplerini karakterize ettim. Glypican 3 ve 5 proteinlerinin interfazdaki ve sitokinezdeki etkileşim partnerlerini, yakınlık bazlı kütle spektrometrisi analiziyle ortaya çıkarttık. Çalışmamız, Glypican 5 proteininin kortikal aktin stabilitesi ve iğ kalıntısı kesilmeside (midbody abscission) önemli rolleri olabileceğini ortaya çıkarmıştır. Bunun yanında, Glypican 3 ve 5 proteinlerinin etkileşim partnerlerinin analizi, bu proteinlerin sitokinezdeki rollerinin anlaşılması açısından önemli ipuçları vermektedir.

AKNOWLEDGEMENTS

Foremost, I would like to thank my advisor Assoc. Prof. Dr. Nurhan Özlü for giving me the opportunity to start my scientific career in her laboratory. Likewise, I would like to thank Prof. Ulrike Eggert for having me in her laboratory. I am very grateful to both for all their patience, constructive criticism, help, and support during my master studies.

In addition, I would like to thank my thesis committee member Asst. Prof. Dr. Ayşe Koca Çaydaşı for their critical reading of my thesis and for their comments.

I am grateful to Dr. Nazan Saner and Dr. Elisabeth Storck Saha for their time, support, and encouragement. I would like to thank them for sharing their knowledge and experience with me. I am very grateful to them for being very understanding and patient when I made mistakes and guiding me to the right path again.

I acknowledge the financial support of the Scientific and Technological Research Council of Turkey (TÜBİTAK) and Koç University during my master education and research.

I acknowledge the Proteomics Facility of Koç University and I would like to thank Büşra Akarlar for her superior technical support with mass spectrometry. In addition, I acknowledge Cellular and Molecular Imaging Core of Koç University Research Center for Translational Medicine (KUTTAM-CMIC) funded by the Republic of Turkey Ministry of Development.

I am very thankful for all former and present members of NozluLab in Koç University and Eggert Group at King's College London. I have learned a lot from each one of them.

I would like to specially thank Altuğ for always being available when I needed him both as a colleague and as a friend, for all his support and patience. My master education will not be as fun without him. I would like to thank him for dealing with all my crises, for sharing his intellectual wisdom, for never judging me for my dark sense of humour. I am very thankful to him for never being rude when I annoyed him the most with my endless speeches. I am very lucky to get to know him and he will be one of my best friends for the rest of my life.

I specially thank Fatmanur, aka Fat, and Umut for being the best housemates ever. I am very grateful for all their love and support during the hardest times. I would like to thank them for all the Sunday breakfasts, hair dying sessions, and endless chats on our beloved kitchen benchtop. Similarly, I would like to thank Çağla for criticizing me a lot on the same benchtop, I know that everything that she says is only because she cares for me deeply.

I would like to thank Tuğçe and Beste for their support during my studies and their beautiful friendship. I would like to thank Hüseyin for all the fun times we had together!

I would like to thank Burak, Burcu, Dilay, Doruk, and Fat (again) for being my family by choice. We have been through a lot together, thank you for always making me feel loved and being there for me no matter what.

I am very grateful for my Jedi Masters Çağakan and Tuğrul for never letting me feel alone during my time in London. I will always owe them a pint of "Neck Oil" even though I will never fully understand why people willingly drink a beverage called like that.

I would like to thank my dearest Mert, for all his love and support. I deeply appreciate the sleepless nights he spent with me while I wrote my thesis. I would like to thank him for reminding me that all the good things happen instantly!

Lastly, I would like to thank my mother Sakine, my father Hakan, and my sister Işıl to whom this thesis is dedicated to. I feel extremely lucky to have them in my life and I am very grateful for their love, support, and encouragement during my scientific career.

TABLE OF CONTENTS

List of Tables 1
List of Figures 2
Abbreviations 4
Chapter 1: Introduction 7
Chapter 2: Literature Review 9
2.1 Regulation of the Cell Cycle 9
2.2 Cytokinesis 11
2.3 Glypicans 13
2.3.1 Glypican 5 16
2.3.2 Glypican 3 18
Chapter 3: Materials and Methods 21
3.1 Cell Culture Conditions and Synchronization Methods 21
3.2 Cloning of HA-GPC3 and cMyc-GPC5 to pENTR1A no ccDB (w48-1) Plasmids 21
3.3 Cloning of HA-EGFP-GPC3, cMyc-EGFP-GPC5, HA-HRP-GPC3, and cMyc-HRP-GPC5 to pENTR1A plasmids via Gibson Assembly 23
3.4 Cloning of HA-GPC3, HA-EGFP-GPC3, HA-HRP-GPC3, cMyc-GPC5, cMyc-EGFP-GPC5, and cMyc-HRP-GPC5 in pENTR1A to pLenti CMV Hygro DEST plasmids 25
3.5 Transfection and Lentiviral Transduction 26
3.6 Generation of Inducible CRISPR-Cas9 System Targeting GPC5 27
3.7 RT-qPCR 27
3.8 HRP-Based Proximity-Dependent Biotinylation and Affinity Capture of Biotinylated Proteins 27
3.9 Proteomic Profiling of Proximity Interaction Partners of GPC3 and GPC5 28
3.10 Western Blotting and Immunostaining 29

3.11 Microscopy and Quantification 32
Chapter 4: Results 33
4.1 GPC3 And GPC5 Enrich at The Cleavage Furrow During Cytokinesis .. 33
4.2 Knocking Out GPC5 Causes Defects in Cell Division 36
4.2.1 Knockout of GPC5 Leads to Multinucleation 36
4.2.2 GPC5 Knockout Does Not Affect the Localization of Certain Proteins Involved in Cytokinesis 39
4.2.3 GPC5 Knockout Causes Defects at Different Stages of Cell Division 41
4.3 Identification of the Interaction Partners of GPC3 and GPC5 47
4.3.1 HRP-Based Proximity Labelling 48
4.3.2 Interaction Partners of GPC5 53
4.3.3 Interaction Partners of GPC3 During Cytokinesis 60
Chapter 5: 64
Discussion 64
Bibliography 67
VITA 70

LIST OF TABLES

Table 2. 1: Tissue expressions and disease associations of glypican family proteins*. 15
Table 3. 1: Western blotting antibodies and dilutions. 30
Table 3. 2: Immunostaining antibodies and dilutions. 31
Table 4. 1: Samples analyzed by LC-MS/MS. 58
Table 4. 2: Numbers of significantly enriched proteins identified by SAINT analysis. 59
Table 4. 3: Cellular localizations and functions of interaction partners of GPC5 during cytokinesis. 61
Table 4. 4: Relative strength of interaction between GPC5 and the common interactors during interphase and cytokinesis 65
Table 4. 5: Cellular localizations and functions of interaction partners of GPC3 during cytokinesis. 67

LIST OF FIGURES

Figure 2. 1: An overview of cell cycle stages and proteins involved in cell cycle regulation. 10
Figure 2. 2: An overview key stages of mammalian cytokinesis. 11
Figure 2. 3: Phylogenetic comparison of Glypicans based on protein sequence homologies 13
Figure 2. 4: Illustration of cleavage sites of Glypicans. 14
Figure 2. 5: Opposing effects of GPC3 and GPC5 in Hedgehod signaling. 17
Figure 2. 6: Inhibitory effects of GPC5 in Wnt/β-catenin signaling. 18
Figure 2. 7: Modulatory role of GPC3 in Wnt signaling in HCC. 19
Figure 4. 1: GPC3 enriches at the cleavage furrow during cytokinesis. 34
Figure 4. 2: GPC5 enriches at the cleavage furrow during cytokinesis. 35
Figure 4. 3: qRT-PCR of Dox inducible GPC5 knock out cells. 36
Figure 4. 4: GPC5 knock out leads to multinucleation in HeLaCas9 GPC5 sg1.8 cells. 37
Figure 4. 5: GPC5 knock out leads to multinucleation in HeLaCas9 GPC5 sg2. 38
Figure 4. 6: Localization of p-myosin in control and GPC5 knock out cells. 39
Figure 4. 7: Localization of Ezrin (A) and p-ERM (B) late telophase in control and GPC5 knock out HeLaCas9 GPC5 sg2 cells. 40
Figure 4. 8: Localization of Anillin (A) and Alix (B) late telophase in control and Dox induced HeLaCas9 GPC5 sg2 cells. 40
Figure 4. 9: Chromosome jiggling phenotype in dividing control and GPC5 knockout cells. 41
Figure 4. 10: Shifted division plane phenotype in dividing control and GPC5 knockout cells. 42
Figure 4. 11: Illustration of shifted division plane phenotype of control and GPC5 knockout cells. 42
Figure 4. 12: Cleavage furrow blebbing phenotype in dividing control and GPC5 knockout cells expressing H2B-mCherry. 43
Figure 4. 13: Quantification of maximal length of cleavage furrow blebbing in control and GPC5 knockout cells. 44

Figure 4. 14: Polar blebbing phenotype in dividing control and GPC5 knockout cells expressing Lifeact-RFP. 45
Figure 4. 15: Quantification of maximal length of polar blebbing in control and GPC5 knockout cells. 45
Figure 4. 16: Live cell fluorescent and bright field imaging of control and GPC5 knockout cells expressing H2B-mCherry. 46
Figure 4. 17: Quantification of abscission time of control and GPC5 knockout cells. 46
Figure 4. 18: Illustration of HRP insertion site and resulting proteins of HRP-tagged GPC3 and GPC5 constructs. 47
Figure 4. 19: Representative microscopy images of HeLa cells expressing cMyc-HRP-GPC5 (left) and HA-HRP::GPC3 (right). 48
Figure 4. 20: Western blotting analysis of HeLa cells expressing cMyc-HRP::GPC5 (left) and HA-HRP::GPC3 (right). 49
Figure 4. 21: Western blotting analysis of Streptavidin enrichment of HeLa Kyoto and HEK293T cells transfected with myc-HRP-GPC5 (left) and HA-HRP-GPC3 (right panel) constructs, respectively. 50
Figure 4. 22: Venn diagram showing the common GPC5 interactors in HEK293T cells. 53
Figure 4. 23: Network clustering of interaction partners of GPC5 during cytokinesis 58
Figure 4. 24: Network clustering of interaction partners of GPC5 at interphase. ... 58
Figure 4. 25: Venn diagram showing the common GPC3 interactors in interphase and in cytokinesis of HEK293T cells. 60
Figure 4. 26: Network clustering of interaction partners of GPC3 during cytokinesis. 63
Figure 4. 27: Common Interaction Partners of GPC3 and GPC5 during cytokinesis 63

ABBREVIATIONS

ABC	Ammonium Bicarbonate
ACN	Acetonitrile
ALIX	Apoptosis-Linked Gene 2-Interacting Protein X
APC/C	Anaphase Promoting Complex/Cyclosome
ATP	Adenosine Triphosphate
BP	Biotin-Phenol
BSA	Bovine Serum Albumin
Cas9	CRISPR Associated Protein 9
CDK	Cyclin Dependent Kinase
CNS	Central Nervous System
CRC	Colorectal Cancer
CRD	Cysteine-Rich Domain
CRISPR	Clustered Regularly Interspaced Palindromic Repeats
DAPI	4',6-Diamidino-2-Phenylindole
DMEM	Dulbecco's Modified Eagle Medium
DMSO	Dimethyl Sulfoxide
DNA	Deoxyribonucleic Acid
dNTP	Deoxyribonucleotide
DTT	Dithiothreitol
ECL	Enhanced Chemiluminescence
ECT2	Epithelial Cell Transforming 2
EGFP	Enhanced Green Fluorescent Protein
ER	Endoplasmic Reticulum
ERK1/2	Extracellular Signal-Regulated Kinase 1
ERM	Ezrin, Radixin, Moesin
ESCC	Esophageal Squamous Cell Carcinoma
ESCRT	Endosomal Sorting Complex Required For Transport
FBS	Fetal Bovine Serum
G0	Resting State
G1	Gap 1

G2	Gap 2
GAG	Glycosaminoglycan
GDP	Guanosine Diphosphate
GEF	Guanine Nucleotide Exchange Factor
GFP	Green Fluorescent Protein
GO	Gene Ontology
GPC	Glypican
GPI	Glycosylphosphatidylinositol
GTP	Guanosine Triphosphate
H_2O_2	Hydrogen Peroxide
HCC	Hepatocellular Carcinoma
HCE	Human Corneal Epithelial Cell Line
HEK293T	Human Embryonic Kidney 293 Cell Line
HGF	Hepatocyte Growth Factor
HRP	Horseradish Peroxidase
HS	Heparan Sulfate
HSPG	Heparan Sulphate Proteoglycan
ITGB1	Integrin B-1
KO	Knockout
LB	Lysogeny Broth Medium
LC	Liquid Chromatography
LOF	Loss Of Function
LSCC	Lung Squamous Cell Carcinoma
MgcRacGAP	Rac GTPase Activating Protein
MKLP1	Mitotic Kinesin-Like Protein 1
MS	Mass Spectrometry
NSCLC	Non-Small Cell Lung Cancer
OCCC	Ovarian Clear Cell Carcinoma
PBS	Phosphate Buffered Saline
PCR	Polymerase Chain Reaction
PEI	Polyethyleneimine
PSM	Peptide Spectrum Matches

PTK7	Protein Tyrosine Kinase 7 (Inactive)
RFP	Ref Fluorescent Protein
RhoA	Ras Homolog Gene Family, Member A
RIPA	Radioimmunoprecipitation Assay Buffer
ROCK	Rho-Associated Protein Kinase
RT-qPCR	Reverse Transcription Quantitative Polymerase Chain Reaction
SDS-PAGE	Sodium Dodecyl Sulfate - Polyacrylamide Gel Electrophoresis
SGBS	Simpson-Golabi-Behmen Syndrome
STC	S-Trityl-L-Cysteine
TBS	Tris Buffered Saline
WCL	Whole Cell Lysate
WT	Wild Type

Chapter 1:

INTRODUCTION

Cytokinesis is an evolutionarily conserved process in which cellular genetic material (chromosomes) as well as cellular organelles and cytoplasm have been divided into two daughter cells. A proper cytokinesis process requires highly coordinated interactions of cell cycle-related proteins as well as cytoskeletal elements, and inner and outer membrane reorganization [1].

Current opinion holds that cytokinesis starts with the signaling between mitotic spindle microtubules and inner plasma membrane proteins, where central spindle recruits Ect2 (RhoA-GEF) and attach it to the plasma membrane to activate RhoA, Activated RhoA proteins then orchestrate the assembly of contractile ring which is composed of actin filaments, bipolar filaments, myosin II, membrane associated septins, and filament cross linker protein anillin. As the contractile ring starts constricting, central spindle microtubules start forming a structure called midbody. Cytokinesis is terminated by the scission of the constricted plasma membrane by ESCRT-III proteins [2].

Most of the scientific knowledge about the key players involved in cytokinesis is restricted to intracellular proteins. Therefore, when Eggert Group (King's College London) discovered in an RNAi screen that cell surface proteins Glypicans 3 and 5's depletion led to cytokinesis failure in cultured cells (data not published), it was interesting as no other extracellular proteins have been implicated in cytokinesis before.

Glypicans (GPCs) belong to a family of cell surface heparan sulfate proteoglycans (HSPGs). There are 6 members of Glypican family proteins: GPC1-GPC6. GPC1,2,4, and 6, and GPC3 and 5 are further sub-grouped based on sequence homologies. All Glypican proteins have 3 main structural components: An N-terminal core protein domain, an inner heparan sulfate chain binding domain, and a C-terminal

glycosylphosphatidylinositol (GPI) anchor site. GPI anchor is the only linkage that attaches Glypicans to outer plasma membrane [3].

Glypicans interact with wide range of proteins including growth factors, plasma membrane enzymes and receptors, morphogens, extracellular matrix proteins, chemokines, and cytokines. Through these interactions, they have exceptional roles in regulating cellular differentiation and tissue reorganization, and many developmental processes. Glypicans' playing significant roles in cancer progression by regulating the activities of these proteins has been shown in many studies [4]. However, the regulatory roles of Glypicans vary among different cell types and developmental stages: A particular Glypican might facilitate the activation of some cellular signaling pathways by stabilizing cell surface receptor interactions in certain cell types and it might as well inhibit the same pathway by competing for the receptor occupancy in others [5]. Therefore, in this thesis I aimed to identify cellular localizations of Glypicans 3 and 5 during cell division, analyze the behavior of the GPC5 knockout cells during cell division, and identify the interaction partners of Glypicans 3 and 5 to provide significant insights about their roles in cytokinesis.

Chapter 2 contains a detailed literature review about the concepts related to this study. The materials and methods used in this study is described in Chapter 3. The results and the interpretations of the findings are presented in Chapter 4. The discussion of the results and future directions of the study are provided in Chapter 5.

Chapter 2:

LITERATURE REVIEW

2.1 Regulation of the Cell Cycle

The cell cycle is a complex sequence of events that the growth and reproduction of almost living species depend on. In this fundamental property of life, cells grow, duplicate their genetic material, and eventually divide into two daughter cells. [6] Cell cycle consist of 4 main stages: G1, S, G2, and M. In Gap 1 (G1) phase, cells prepare themselves for DNA replication by growing, increasing the number of their organelles, and synthesizing new macromolecules such as proteins, and RNAs. G1 phase is followed by S phase where DNA replication occurs. After successful DNA replication, cells go into Gap 2 (G2) phase where the cell prepares itself for mitosis (M) where the replicated DNA and cellular material are divided into two daughter cells (**Figure 2.1**). Some cells in G1 phase might enter G0 phase, where the cells are quiescent and not committed to DNA replication or proliferation [7]. M phase is also composed of 4 different stages: prophase, metaphase, anaphase, and telophase. Equal separation of the genetic material to two daughter cells is completed by a successful cytokinesis in which the dividing cell is physically separated [8].

Cell cycle progression is strictly regulated at many levels by various proteins (Figure 2.1). After the restriction point (R) in G1 in which the cell is committed to cell cycle entry, there are three main checkpoints that ensure the cell cycle proceeds successfully in an orderly fashion. These checkpoints are G1-S checkpoint, G2-M checkpoint, and mitotic spindle checkpoint. G1-S and G2-M checkpoints arrest the cell cycle to ensure that DNA is not damaged and provide time to repair when necessary. G1-S checkpoint resides before the S phase where p53-dependent cell cycle arrest is induced if DNA damage is detected. Similarly, at G2-M checkpoint, entry into mitosis is prevented by Cdc25 regulated cascade of events if DNA damage is detected (**Figure 2.1**). Finally, cell cycle

can be arrested in metaphase at mitotic spindle checkpoint if improper alignment of chromosomes is detected [7, 9].

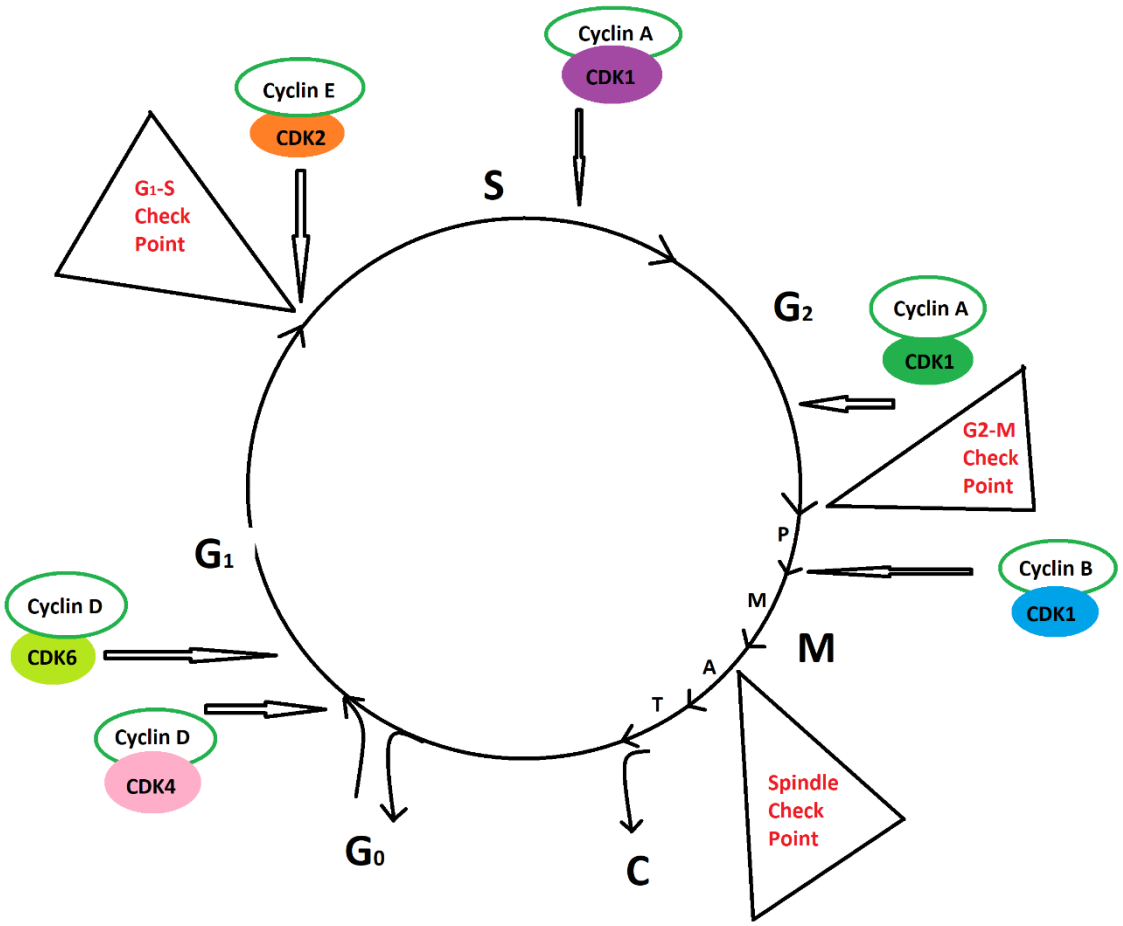

Figure 2. 1: An overview of cell cycle stages and proteins involved in cell cycle regulation.

(Adapted from [10])

The main regulators of cell cycle progression are family of kinases called Cyclin-Dependent Kinases (CDKs) and their activating proteins cyclins. As their name implicates, cyclin levels oscillate inside the cell during the cell cycle where CDK levels stay stable. This is the main mechanism behind the cell cycle regulation. In the different phases of the cell cycle, different cyclin protein and their corresponding CDKs are activated. For example, CDK4 and CDK6 proteins can be activated by Cyclin D to induce G0/G1 transition. G1/S transition is regulated by the activity of CDK2-Cyclin E complex

whereas S phase is regulated by the activity of CDK2-Cyclin A complex and their downstream effectors. Entry into mitosis is controlled by the activity of CDK1-Cyclin A complex and CDK1-Cyclin B complex monitors and regulates mitosis [10]. Mitotic exit is achieved by the degradation of Cyclin A and Cyclin B proteins by Anaphase Promoting Coplex/Cyclosome (APC/C) after the cell passes the mitotic spindle checkpoint as mentioned before. Together with other kinases, phosphatases and regulatory proteins, this cascade of events that are very briefly described here eventually comes to an end with the induction of cytokinesis [11].

2.2 Cytokinesis

Cytokinesis is the last stage and therefore the end of the cell cycle in which two daughter cells bearing the equal amount of genetic material are physically separated. In mammalian cells, cytokinesis can be mainly described in four stages: The determination of the cleavage plane, cleavage furrow ingression, midbody formation, and abscission (cleavage) of the midbody **(Figure 2.2)** [12, 13].

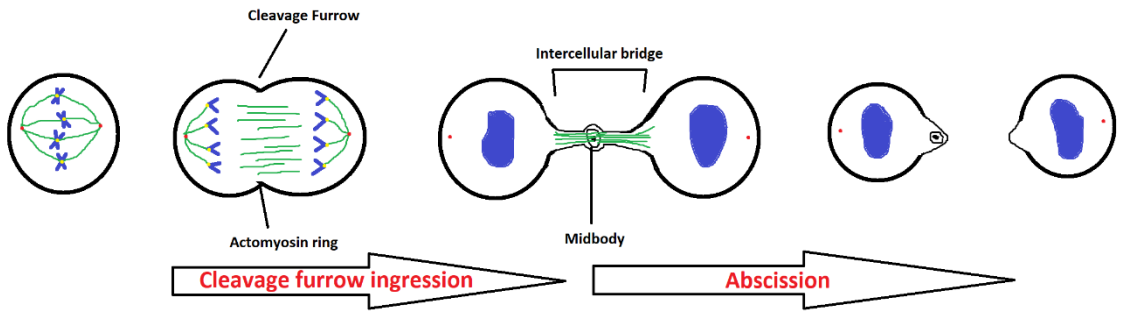

Figure 2. 2: An overview key stages of mammalian cytokinesis.

Mammalian cytokinesis starts with determination of the cleavage furrow; followed by cleavage furrow ingression and ends abscission (Adapted from [12]).

Cytokinesis starts with the determination of the cleavage plane. Cleavage plane determines the site where the cytokinesis machinery will be recruited. The correct positioning of the cleavage plane is controlled by the communication between the actin cortex and the central spindle microtubules. One of the main players reside on the spindle microtubules is Centralspindlin complex that is composed of RhoGAP/MgcRacGAP and

MKLP1. Centralspindlin complex creates a docking station for RhoA activating protein ECT2 that remains autoinhibited until late anaphase. The docking of ECT2 release its autoinhibition via the activity of MKLP1. In the active conformation, ECT2 activates RhoA by acting as a Rho-GEF promoting the exchange of GDP to GTP on RhoA [2].

The second stage of cytokinesis, cleavage furrow ingression, is mediated by active RhoA (RhoA-GTP). After activation by ECT2, RhoA-GTP induces actin nucleation and polymerization by activating formins by relieving their autoinhibition. In addition, RhoA-GTP stimulates Myosin-II phosphorylation at its regulatory light chain by activating ROCK and Citron kinases. The organization and activation of actomyosin ring at the cleavage plane initiates cleavage furrow ingression. Anillins and septins also play crucial roles in the initiation of cleavage furrow ingression by acting as scaffolds and binding F-actin, myosin-II, and RhoA-GTP [13].

Midbody formation is the third stage of cytokinesis where cleavage furrow ingression reaches to 1-1.5 microns in diameter. At this stage, dynamic F-actin is lost [14] however many other proteins involved in earlier stages of cytokinesis stays around/at the midbody. For example, Centralspindlin complex recruited by PRC1 protein is necessary formation of the midbody. Moreover, it additionally involves in the recruitment of abscission proteins to the midbody [8].

At the last stage of cytokinesis, abscission, midbody is cleaved and the cell splits into two daughter cells. Abscission of midbody is catalyzed by ESCRT-III proteins where they form a spiral-shaped membrane associated polymers. Many other midbody associated proteins involve in the recruitment of ESCRT-III to the midbody and formation of the spiral polymers such as Cep55, ESCRT-I, ALIX, and many others. After the cleavage, the remnant of the midbody stays with either one of the daughter cells. [2, 15]

2.3 Glypicans

Glypicans (GPCs) are members of Heparan Sulphate Proteoglycans (HSPGs) that are highly conserved among across eukaryotes (**Figure 2.6)** [16]. They are predominantly found on the exocytoplasmic surface of the plasma membrane where they are covalently docked to the membrane via GPI anchors.

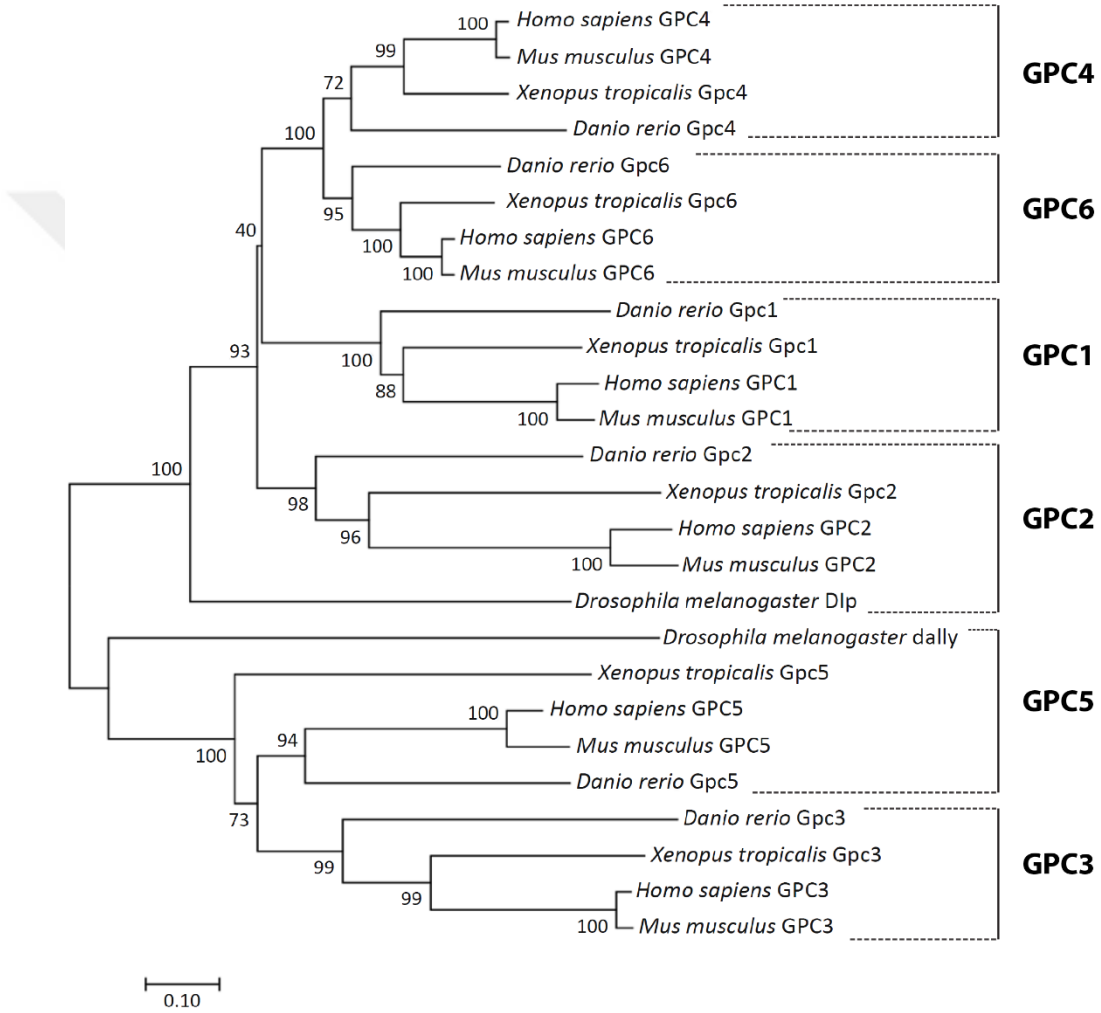

Figure 2. 3: Phylogenetic comparison of Glypicans based on protein sequence homologies.

Glypicans can be grouped into two subfamilies: GPC1/2/4/6 and GPC3/5. Two D. melanogaster Glypicans are Dally and Dally-like protein (Dlp) which are orthologs of GPC3/5 and GPC1/2/4/6, respectively (Adapted from [16]).

There are six members of Glypican family proteins namely GPC1-GPC6. All glypicans carry an N-terminal secretory signal sequence and a putative C-terminal sequence necessary for GPI anchor attachment. Glypicans are thought to share a similar 3D structure due to the presence of 7 disulfate bridges created by 14 conserved cysteine residues [17]. In addition, all 6 members of Glypicans carry conserved sites for glycosaminoglycan (GAG) chains near their membrane attachment points. These motifs are necessary for Heparan Sulphate (HS) attachments [18]. Some glypicans might be subjected to endoproteolytic cleavage by Furin-like convertases that might generate two subunits remain attached by disulfide bridges or they can be cleaved and by the lipase Notum and be secreted to the extracellular space (**Figure 2.4**) [19-22]

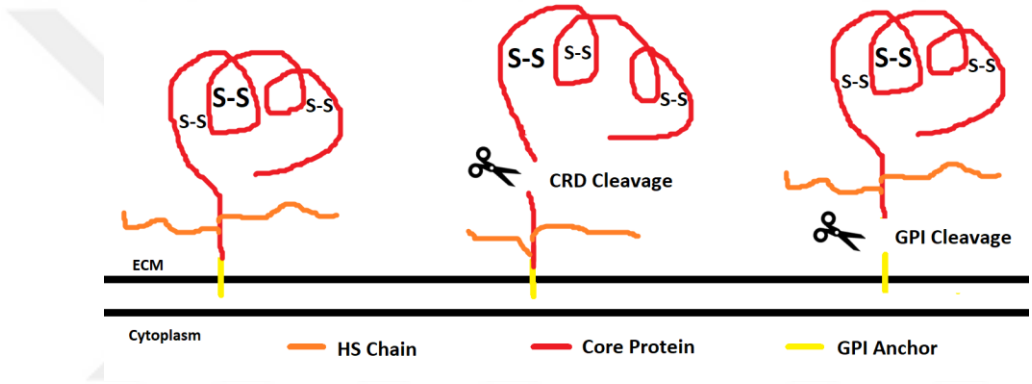

Figure 2. 4: Illustration of cleavage sites of Glypicans.
A representative illustration of Glypicans including core protein, HS binding sites, and GPI anchor (Left). Glypicans can be secreted by endoproteolytic cleavage near the cysteine-rich domains (CRD) or at the GPI anchor sites (Adapted from [20]).

Glypicans interact with wide range of molecules and proteins mostly due to (but not restricted to) the diversity of modifications on their HS chains. Since they explicitly face the extracellular environment, they can regulate developmental processes, cellular differentiation and tissue reorganization and many signaling pathways by interacting with ligands such as morphogens, growth factors, enzymes, receptors, extracellular matrix proteins, cytokines, and chemokines [4, 17]. Due to their wide range of ligands, glypicans have been shown to be involved in many types of cancers and other diseases summarized in *Table 2.1*. The differential expression patterns of glypicans in various types of cancers allow them to act as both tumor suppressors and oncogenes. This dual activity of glypicans is mostly depend on the type cells as well as the stage of cancer [4, 17, 18, 20, 23, 24].

Table 2. 1: Tissue expressions and disease associations of glypican family proteins*.

GPC[1]	**Tissue Expression**		**Disease**		
	Embryonic Stage	**Adult**	**Upregulated**	**Downregulated**	**LoF**[8]
GPC1	CNS[2], bone, kidney, muscle	Ubiquitous	Pancreatic Cancer, Breast Cancer, Gliomas, ESCC[3], CRC[4], Mesothelioma, Prostate cancer		
GPC2	CNS	Undetected	Pediatric cancers		
GPC3	Ubiquitous	Ovaries, breast, lung, kidney	HCC[5], LSCC[6], Cervical Cancer, Ovarian Clear Cell Carcinoma	**Breast cancer, Mesothelioma, Renal cancer, Stomach cancer, Ovarian cancer,**	**SGBS**[7]
GPC4	CNS, adrenal cortex, kidney, lung	Ubiquitous	Pancreatic Cancer		
GPC5	CNS, kidney, lung, limbs, liver	CNS	Rhabdomyosarcoma, Salivary adenoid cystic carcinoma	Lung cancer, Prostate cancer, Glioma,	
GPC6	Several tissues	Several tissues	Breast cancer, Ovarian cancer		Omodysplasia

*: Adapted from [4]. [1-8]: GPC: Glypican; CNS: Central Nervous System; ESCC: Esophageal Squamous Cell Carcinoma; CRC: Colorectal Cancer; SGBS: Simpson-Golabi-Behmen Syndrome; HCC: Hepatocellular Carcinoma; LSCC: Lung Squamous Cell Carcinoma; LOF: Loss of Function.

2.3.1 Glypican 5

GPC5 gene is located at 13q31.3 covering 1.47 Mb wide genomic region [25]. GPC5 is a 572 amino acid long protein that has five predicted HS attachment sites closer to its C terminus at S441, S486, S495, S507, and S509. At the embryonic stage GPC5 is expressed in the CNS, kidneys, lungs, limbs, and liver at the embryonic stage. GPC5 expression is enriched in CNS system in adults [4, 25, 26].

Previous studies revealed that GPC5 can be linked to many types of diseases. For example, two previous studies have been separately confirmed that GPC5 mRNA levels are increased due to *GPC5* gene amplification in rhabdomyosarcoma (RMS) suggesting that *GPC5* expression might play an oncogenic role in RMS [17, 27, 28]. In addition, the oncogenic role of GPC5 has been further shown in lung metastasis of salivary adenoid cystic carcinoma [29].

Other studies, however, revealed more interesting findings. One study showed a single-polypeptide polymorphism in the *GPC5* gene might be associated to increased susceptibility to lung cancer [30, 31]. This finding was also supported by another study in which GPC5 expression was decreased in non-small cell lung cancer (NSCLC) and metastatic properties of these cells have been reversed with the overexpression of *GPC5* [31]. Yet another study also confirmed that GPC5 expression was decreased due to hypermethylation of GPC5 promoter in NSCLC [31, 32]. Although these studies suggest that GPC5 might have a role as a tumor suppressor in lung cancer, contradicting results have also been published. For example, one study showed an increased expression of in NSCLC that has been associated with lower survival rates [17, 33].

The contradicting findings in the case of NSCLC might be restricted to this type of cancer. However, the oncogenic effect of *GPC5* observed in RMS and salivary adenoid cystic carcinomas has not been observed in other cancer types. Interestingly, several studies speculated a possible tumor suppressor role of GPC5 due to reduced *GPC5* expression in many cancers such as breast cancer [34], prostate cancer [35], pancreatic cancer [36], hepatocellular carcinoma (HCC) [37], and glioma [38] compared to healthy controls [4, 17].

One reason behind the opposing effects of GPC5 on different types of cancer might be due to the contribution its interactors on the cell surface. GPC5's involvement in the regulation of different signaling pathways such have been previously shown in previous

research. While the oncogenic effect of GPC5 in RMS has been shown to be achieved by promoting Hedgehog signaling by stabilizing and therefore facilitating the binding of Hh to Patched (**Figure 2.5**) [19, 39], in other cancer types, GPC5's acting as a tumor suppressor has been associated to its inhibitory roles in Wnt/β-catenin signaling where GPC5 sequestering Wnt3a ligands therefore inhibiting their finding to Frizzled receptor (**Figure 2.6**) [40].

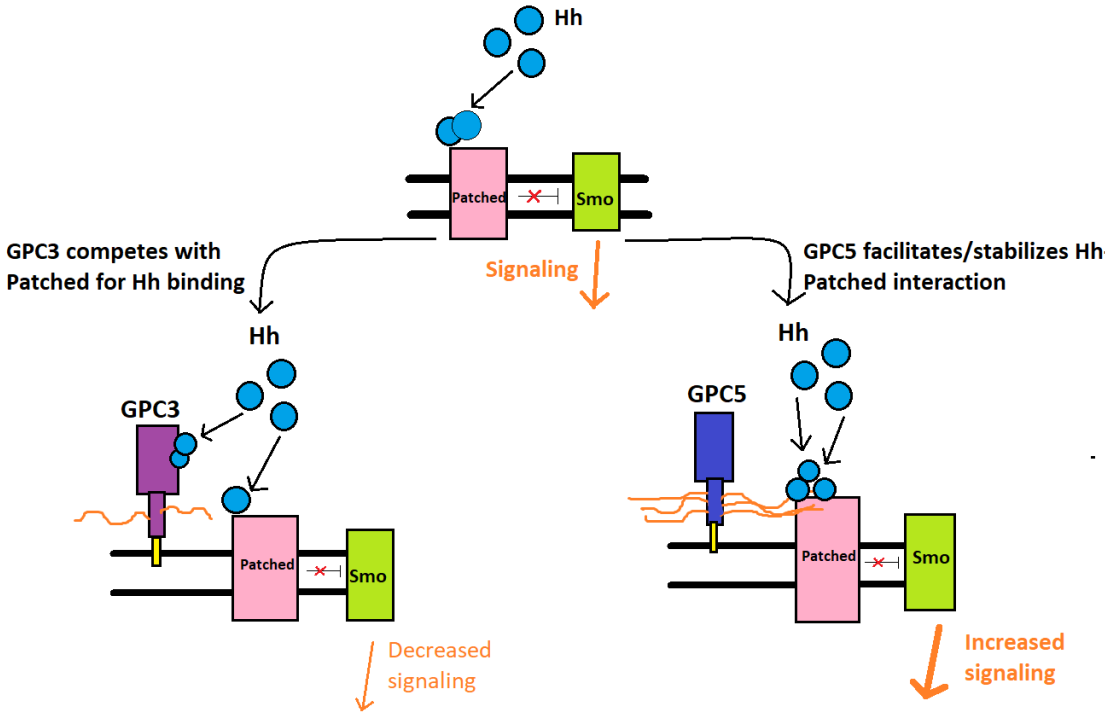

Figure 2. 5: Opposing effects of GPC3 and GPC5 in Hedgehod signaling.

An illustration of the opposing effects of Glypican 3 and Glypican 5 in Hedgehog signaling pathway. GPC3 decrease Hedgehog signaling by competing Patched receptor for Hedgehog binding. GPC5 increase Hedgehog signaling by facilitating and stabilizing the interaction between Hedgehod-Patched interaction (Adapted from [19]).

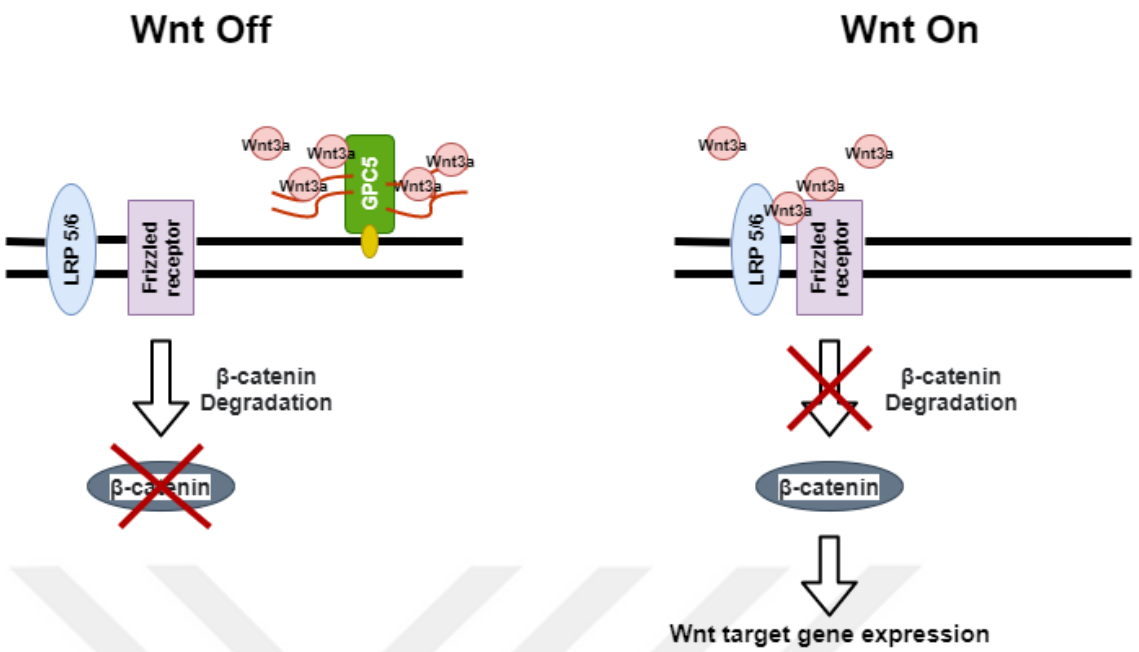

Figure 2. 6: Inhibitory effects of GPC5 in Wnt/β-catenin signaling.

A model proposed by Li et al. describing the inhibitory effects of GPC5 in Wnt3a signaling by sequestering Wnt3a molecules and therefore competing with Frizzled receptor for Wnt3a binding (Adapted from [40]).

2.3.2 Glypican 3

GPC3 is the most well-studied one of all Glypicans. 580-amino-acid long GPC3 protein is encoded by the *GPC3* gene that is located on Xq26. Unlike GPC5, which has five predicted HS binding sites near its C-terminus, GPC3 has two predicted HS binding sites at S495 and S509. Three isoforms of resulting in alternative splicing of GPC3 have been detected [41]. Although GPC3 expression has been detected in livers, lungs, kidneys, and placenta in embryonic stage and during development, the expression levels drop significantly in adults in adult tissues [4, 17].

GPC3 has been linked to many diseases, especially to various types of cancers, due to its modulatory roles in many signaling pathways such as Hedgehog [19, 42], Wnt/β-catenin [42, 43], and HGF [43]. GPC3 overexpression has been linked to many cancer types such as hepatocellular carcinoma (HCC) [23], lung squamous cell carcinoma (LSCC) [44], melanoma [45, 46], ovarian clear cell carcinoma (OCCC) [46], thyroid cancer [47], and many others. In contrast, just like GPC5, potential tumor suppressor effects of GPC3 have also been revealed in many studies. Among those, Simpson-Golabi-

Behmel overgrowth syndrome (SGBS) is one of the most well-studied diseases caused by a loss-of-function mutation in *GPC3* [48]. Decreased *GPC3* expression has been linked to several cancer types including breast cancer [49], mesothelioma [50], and renal cell carcinoma [51].

The involvement of GPC3 in HCC is one of the most well-studied diseases in GPC3 research. Unlike the effect of GPC5 in Wnt signaling, many studies show that GPC3 might attract Wnt ligand to the plasma membrane and stabilize Wnt-Frizzled interaction **(Figure 2.7)** [17]. Due to the strong correlation of the overexpression of GPC3 in HCC, GPC3 is being used both for diagnostic [52] and therapeutic purposes in the recent years [23, 53, 54].

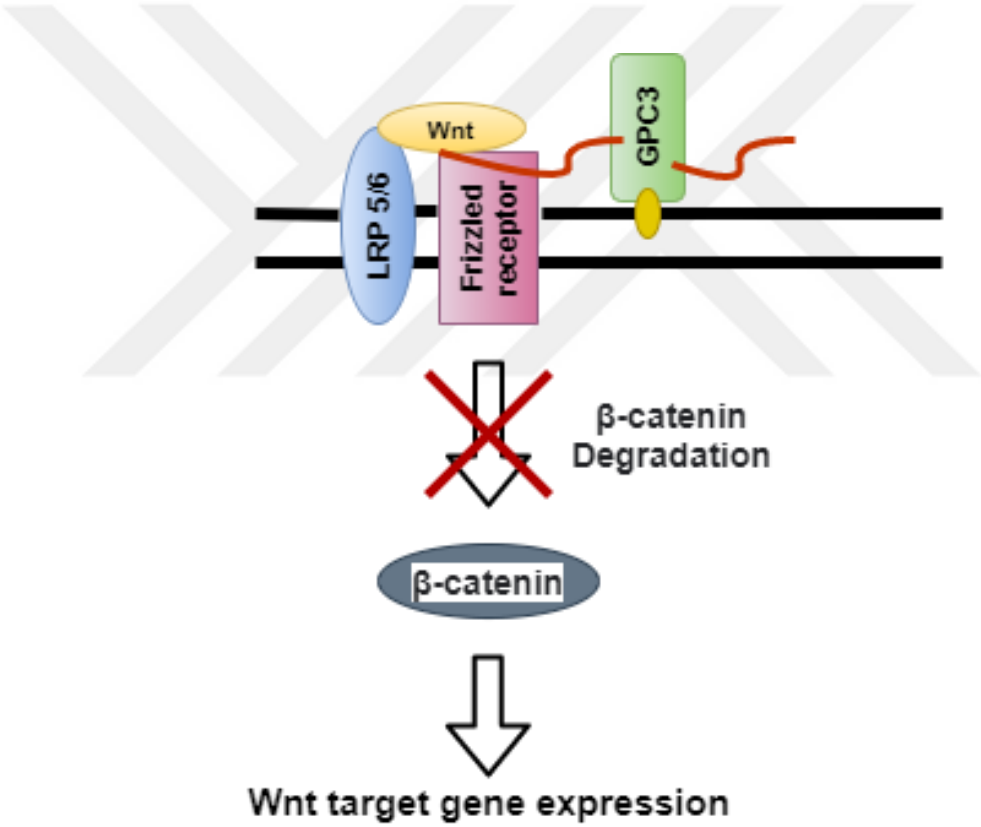

Figure 2. 7: Modulatory role of GPC3 in Wnt signaling in HCC.

An illustration explaining the modulatory role of GPC3 in Wnt signaling in HCC cells. GPC3 facilitates Wnt and Frizzled receptor binding by facilitating the interaction between the ligand and the receptor (Adapted from [17]).

Another very well-studied case of GPC3-related diseases is Simpson-Golabi-Behmel Syndrome (SGBS). The loss-of-function mutation in *GPC3* causing SGBS is shown to be the cause of hyperactive Hedgehog signaling pathway [22, 55]. Multiple studies revealed that the loss of Hh ligand sequestration in the malfunction of GPC3 because functional GPC3 act as a competitor for Patched for Hh ligand binding (**Figure 2.9**) [3, 56].

Overall, many studies have shown the effects of both oncogenic and suppressive effects of Glypicans 3 and 5 many types of cancers and other diseases. These findings suggest important roles of Glypicans 3 and 5 in regulation of cell proliferation through their interaction partners. However, their individual roles in cytokinesis in molecular and cellular levels are not well-studied. Furthermore, RNAi screens carried out in Eggert Group (King's College London) revealed a significant increase in multinucleated cells in the knock-down of Glypicans 3 and 5 (Data not published). Therefore, in this study we aimed to identify the roles of Glypicans 3 and 5 during cytokinesis in order to understand their roles in cell division.

Chapter 3:

MATERIALS AND METHODS

3.1 Cell Culture Conditions and Synchronization Methods

HeLa and HEK293T cells were grown in Dublecco's Mininum Essential Medium supplemented with 10% FBS (Fetal Bovine Serum) and 1% Penecillin/Streptomycin in 37˚C incubator buffered with 5% CO_2. Doxycycline inducible GPC5 knock down HeLa cells were grown Dublecco's Minimum Essential Medium supplemented with 10% tetracycline-free FBS (631367, Takara) and 1%PS in 37˚C incubator buffered with 5% CO_2.

For cytokinesis arrest, cells were treated with 2 mM 2'-Deoxythymidine (DB0049, BioBasic) for 18 hours followed by a 8-hour release, twice. After the last release, the cells were treated with 10 ng/ml of nocodazole (487928, Calbiochem) for 5 hours for mitotic arrest. After 5 hours the cells were washed 3 times with PBS and incubated in DMEM (10% FBS, 1% PS) until majority of the cells undergo cytokinesis by checking them in every ten to fifteen minutes.

Alternatively, after double thymidine treatment inducing monomopolar cytokinesis arrest was achieved by treating the cells with 10 µM STC (164739, Sigma-Aldrich) in complete DMEM for 12 hours and a following 15 minutes 100µM Purvanol A (1580, Tocris Bioscience) treatment.

3.2 Cloning of HA-GPC3 and cMyc-GPC5 to pENTR1A no ccDB (w48-1) Plasmids

HA-tagged human GPC3 was ordered from Addgene (#24670). In order to clone HA-tagged GPC3 gene into pENTR1A no ccDB (w48-1) vector (Addgene, # 17398), EcoRI and XhoI restriction sites were added to N- and C- terminus of HA-tagged GPC3 (Addgene #24670) via PCR respectively (10.0 ul 5X Phusion HF Buffer, 1.0 ul 10mM dNTPs, 2.5 ul 10µM forward and reverse primers, 2.0 ul of template

DNA (10 ng/ul), 0.5 ul Phusion HF DNA Polymerase (M0530S, NEB), 31.5 ul ddH_2O. The primer pairs used for each reaction were EcoRI_GPC3_fwd: 5'-GCTAGAATTCAGGATGGCCGGGACCGT -3' and XhoI_GPC3_rev: 5' – GCTACTCGAGCAGTCAGTGCACCAGGAAGAAG – 3'. PCR conditions: Initial denaturation 98˚C – 30 seconds, Denaturation 98˚C – 10 seconds, annealing temperature 69˚C – 20 seconds, Extension 72˚C – 30 seconds, Final extension 72˚C – 7 min, 30 cycles.) The resulting PCR product (HA-GPC3) was run on 1% agarose gel at 90V for 50 minutes and was purified by NucleoSpin® Gel and PCR Clean-up Kit (740609, Machare-Nagel) following manufacturer's instructions. Then PCR product and pENTR1A no ccDB (w48-1) vector were digested by EcoRI-HF (NEB #R3101) and XhoI (NEB # R0146S) enzymes (5.0 ul CutSmart® Buffer, 2.0 ul EcoRI-HF enzyme, 2.0 ul XhoI enzyme, 1.0 ug DNA (HA-GPC3 PCR product or pENTR1A no ccDB (w48-1) vector, and ddH_2O until final volume reached 50.0 ul. The mixtures were incubated at 37˚C for 3 hours) Digested DNAs were run on 1% agarose gel at 100V for 40 minutes and was purified by NucleoSpin® Gel and PCR Clean-up Kit (740609, Machare-Nagel) and were ligated in 3:1 insert:vector ratio (10.0 ul 2X Quick Ligase Buffer, 26.0 ng digested pENTR1A vector, 61.0 ng digested HA-GPC3 produc, 1.0 ul Quick Ligase, and 5.5 ul ddH_2O). Ligation reaction mix were incubated at room temperature for 15 minutes and then was chilled on ice.

5 ul of reaction mixture was used to transform chemically competent *E.coli* DH5α bacterial cells. Transformation was carried out by incubating ligation-product-added competent bacteria sample for 30 minutes on ice, transferring the sample to 42˚C for 45 seconds to perform heat shock, andfinally incubating the sample on ice again for 2 minutes. 950.0 ul of liquid LB media was added onto the competent cells and the sample was incubated at 37C for 1.5 hours on a 300 rpm shaker. Then, the tube was centrifuged at 7000 rpm for 30 seconds, 850.0 ul of supernatant was discarded, remaining 150.0 ul was used to resuspend the pellet. The cells were then plated onto Kanamycin+ LB agar plates. Plates were placed in a 37˚C incubator overnight. The next day, randomly chosen single colonies were inoculated into liquid LB (with Kanamycin) and incubated overnight at 37˚C on 200 rpm rotational shaking. Plasmids were purified by NucleoSpin Plasmid, Mini kit for plasmid DNA (7409588.50, Macherey-Nagel) following the manufacturer's instructions. Samples were checked for proper insertion by restriction digestion using

SacI-HF (NEB # R3156S) and XbaI (NEB #R0145S) enzymes and positive samples were selected.

3.3 Cloning of HA-EGFP-GPC3, cMyc-EGFP-GPC5, HA-HRP-GPC3, and cMyc-HRP-GPC5 to pENTR1A plasmids via Gibson Assembly

For generation of HA-EGFP-GPC3, HA-HRP-GPC3, cMyc-EGFP-GPC5, and cMyc-HRP-GPC5 constructs Gibson Assembly (Isothermal Assembly) method was used. First, 5X ISO Buffer was prepared with 200.0 ul 1M Tris-HCl (pH: 7.5), 10.0 ul 2M $MgCl_2$, 40.0 ul 10mM dNTPs, 20.0 ul 1M DTT, 0.1g PEG-8000, 20.0 ul 100mM NAD, and 110.0 ml ddH_2O. 32.0 ul aliquots were prepared and stored at -20˚C freezer. Gibson Assembly Master Mix was prepared by mixing 32.0 ul 5X ISO Buffer, 1.2 ul T5 Exonuclease (T5-20318, Epicentre) (1:10 Diluted), 2.0 ul Phusion HF DNA Polymerase (M0530S, NEB), 16.0 ul Taq DNA Ligase (M0208S, NEB), and 70.0 ul ddH_2O on ice. 15.0 ul aliquots were prepared on ice in PCR tubes and stored at -20˚C freezer.

Overlapping ends added to HA-GPC3 and cMyc-GPC5 in pENTR1A plasmids at appropriate sites by PCR using specific sets of forward and reverse primers (10.0 ul Phusion GC Buffer, 1.0 ul 10mM dNTPs, 2.5 ul 10µM forward and reverse primers, 1.0 ul of template DNA (10 ng/ul) (cMyc-GPC5 in pENTR1A and HA-GPC3 in pENTR1A were used as template DNAs), 1.5 ul DMSO, 0.5 ul Phusion HF DNA Polymerase (M0530S, NEB), 31.0 ul ddH_2O. The primer pairs used for each reaction were GPC5-EGFP-Forward: 5’-GACGAGCTGTACAAGGGCGGCGGCGTGCAGACCTGCGAAGAAG -3’, GPC5-EGFP-Reverse: 5’-CAGCTCCTCGCCCTTGCTCACTCCAGAGCCGCCCAGATCTTC-3’, annealing temperature 69˚C; GPC3-EGFP-Forward: 5’-GCTGTACAAGGGCGGCTCTGGAAACACCTGTCACCAAGTCCG -3’, GPC3-EGFP-Reverse: 5’-GCTCCTCGCCCTTGCTCACGAGGCTAGCATAATCAGGAACATC -3’, annealing temperature 64˚C; HRP-GPC5-Forward: 5’-GAGTGGTCAACAGCAACTCTGGCGGCTCTGGAGGCG -3’, HRP-GPC5-Reverse: 5’- GTTAACTGCTGGGCCCCCAGATCTTCTTCAGAAATAATTTTTGTTCTCC -3’, annealing temperature 66˚C; HRP-GPC3-Forward: 5’-

CAACAGCAACTCTCCGCGGAGCCTCAACACCTGTCACC -3', HRP-GPC3-Reverse: 5'-CTGCTGGGCCCCTCCAGAGCCGCCAGCATAATCAGGAACATCATAGAGGC -3', annealing temperature 63˚C. PCR conditions: Initial denaturation 98˚C – 30 seconds, Denaturation 98˚C – 10 seconds, Gradient annealing temperature – 20 seconds, Extension 72˚C – 2 min, Final extension 72˚C – 7 min, 30 cycles.)

EGFP and HRP fragments with appropriate overlapping ends amplified from pEGFP-N1 (Clontech #6085-1) and HRP-TM in pLenti CMV Hygro DEST (w117-1) vectors, respectively via PCR using specific primer pairs (10.0 ul Phusion HF Buffer, 1.0 ul 10mM dNTPs, 2.5 ul 10µM forward and reverse primers, 1.0 ul of template DNA (10 ng/ul) (cMyc-GPC5 in pENTR1A and HA-GPC3 in pENTR1A were used as template DNAs), 1.5 ul DMSO, 0.5 ul Phusion HF DNA Polymerase (M0530S, NEB), 31.0 ul ddH_2O. The primer pairs used for each reaction were EGFP-GPC5-Forward: 5'-AAGAAGATCTGGGCGGCTCTGGAGTGAGCAAGGGCGAGGAG-3', EGFP-GPC5-Reverse: 5'-CGCAGGTCTGCACGCCGCCGCCCTTGTACAGCTCGTCCATGCCG -3', annealing temperature 65˚C; EGFP-GPC3-Forward: 5'-GTTCCTGATTATGCTAGCCTCGTGAGCAAGGGCGAGGAGC -3', EGFP-GPC3-Reverse: 5'-CTTGGTGACAGGTGTTTCCAGAGCCGCCCTTGTACAGCTCGTCCATGCC -3', annealing temperature 66˚C; GPC5-HRP-Forward: 5'-CTTATTTCTGAAGAAGATCTGGGGGCCCAGCAGTTAACCC -3', GPC5-HRP-Reverse: 5'- GCACGCCTCCAGAGCCGCCAGAGTTGCTGTTGACCACTCTGC -3', annealing temperature 67˚C; GPC3-HRP-Forward: 5'-GTTCCTGATTATGCTGGCGGCTCTGGAGGGGCCCAGCAGTTAACC -3', GPC3-HRP-Reverse: 5'- GGTGACAGGTGTTGAGGCTCCGCGGAGAGTTGCTGTTG -3' annealing temperature 67˚C. PCR Conditions: Initial denaturation 98˚C – 30 seconds, Denaturation 98˚C – 10 seconds, Gradient annealing temperature – 20 seconds, Extension 72˚C – 15 and 30 seconds for HRP and EGFP fragment amplifications respectively, Final extension 72˚C – 7 min, 30 cycles.)

PCR products were run on 1% agarose gel at 100V for 45 minutes. Reaction products were purified by NucleoSpin® Gel and PCR Clean-up Kit (740609, Machare-Nagel) following manufacturer's instructions.

For Gibson Assembly reaction, corresponding fragments were combined at equal molecular ratio in a PCR tube not exceeding total volume of 5 ul (100 ng of plasmid backbones were used for each reaction). The combined fragments (5 ul) were to the Gibson Assembly Master Mix (15 ul) aliquot and mixed by pipetting. Reactions were placed at 50˚C for 25 minutes. 2 ul of each reaction were used to transform chemically competent *E.coli* DH5α bacterial cells with the transformation protocol described above and spread onto Kanamycin+ LB agar plates. Plates were placed in a 37˚C incubator overnight and randomly chosen single colonies were inoculated into liquid LB (with Kanamycin) and incubated overnight at 37˚C on 200rpm rotational shaking. Plasmids were purified by NucleoSpin Plasmid, Mini kit for plasmid DNA (7409588.50, Macherey-Nagel) following the manufacturer's instructions. Purified plasmids were sequenced with the following primers by Macrogen Company, The Netherlands: (pENTR-F: 5'- CTACAAACTCTTCCTGTTAGTTAG -3', pENTR-R:5'- ATGGCTCATAACACCCCTTG -3', HRP-F: 5'- CTGAATCGCTCGAGTGACCTTG -3', GPC5-F: 5'- CAGGAACATGGCCTTGGAGG -3', GPC3-F: 5'- GCTTATTATGACCCAGGTTTC -3', EGFP-F: 5'- GGGCACAAGCTGGAGTACA -3'.)

3.4 Cloning of HA-GPC3, HA-EGFP-GPC3, HA-HRP-GPC3, cMyc-GPC5, cMyc-EGFP-GPC5, and cMyc-HRP-GPC5 in pENTR1A to pLenti CMV Hygro DEST plasmids

All constructs were cloned into pLenti CMV Hygro DEST plasmid (w117-1) (Addgene #17454) mammalian expression vector via Gateway LR Reaction. For each reaction 100.0 ng of construct in pENTR1A, 100.0 ng pLenti CMV Hygro DEST (w117-1) were mixed with 2.0 ul TE Buffer, 1.0 ul Gateway® LR Clonase® II (11791020, Invitrogen), and ddH2O were mixed to reach final volume of 5 ul. The reaction mixtures were incubated at room temperature overnight. Next day reactions were stopped by adding 0.5 ul Proteinase K (11791020, Invitrogen) and incubating 10 minutes at 37˚C. 2 ul of each reaction were then used to transform chemically competent Stbl3 bacterial cells and were spread onto Ampicillin+ LB agar plates. After plates were incubated in a 37C incubator overnight, single colonies from each plate were picked and were inoculated in liquid Ampicillin+ LB media in a 200rpm rotational shaker at 37C overnight. The next

day, plasmid DNAs were purified by NucleoSpin Plasmid, Mini kit for plasmid DNA (7409588.50, Macherey-Nagel) following the manufacturer's instructions.

3.5 Transfection and Lentiviral Transduction

To perform transfection, cells were seeded targeting 60% confluency on the day of transfection. The next day, cells were washed with PBS twice then added Transfection Enhancement Medium (DMEM containing 1%FBS and 1%PS) and incubated at 37C incubator buffered with 5% CO2 for 30 minutes. Meanwhile, for 1 ug DNA transfection, 1 ul of Lipofectamine™ 2000 Transfection Reagent (11668019, Invitrogen) and 1 ug DNA were diluted in 80 ul OPTI-MEM (31985047, Invitrogen) in 1.5 ml test tubes, separately. The mixtures were incubated at room temperature for 5 minutes. The diluted DNA and diluted Lipofectamine™ 2000 were mixed in a new tube with 1:1 ratio, gently mixed by tapping, and incubated at room temperature for 20 minutes. The mixture was added onto the cells dropwise. Transfection media were replaced with fresh media after 6 hours.

HeLa cells stably expressing myc-HRP-GPC5 or HA-HRP-GPC3 were created via lentiviral transduction. For this procedure, HEK293T cells were seeded onto 100 mm dishes - On the day of transfection cells were 60% confluent. 7.5 µg cMyc-HRP-GPC5 in pLenti CMV Hygro DEST or HA-HRP-GPC3 in pLenti CMV Hygro DEST were mixed with 5 µg psPAX2 (Addgene #12260) and 2.5 µg VSV-G (Addgene #8454) vectors in 750 µl OPTI-MEM (31985047, Invitrogen). 45 µl PEI was added onto the samples (1:3 ratio), the mixtures were vortexed immediately and incubated for 30 minutes at room temperature. After 30 minutes, the mixtures were added onto HEK293T cells dropwise and the cells were incubated overnight in a 37˚C incubator buffered with 5% CO2. The next day, media were replaced with fresh media. After 48 hours viruses were collected, filtered with 0.45 µm filters and stored at -80˚C. For transduction, HeLa cells were seeded in 6-well plate and were given 500 µl of virus. After 48 hours, media were replaced with fresh media containing 300 µg/ml Hygromycin B for selection. Transduced cells were selected until all the cells in the mock treatment were dead.

3.6 Generation of Inducible CRISPR-Cas9 System Targeting GPC5

Inducible CRISPR GPC5 knock out cells were created using the guide RNA's designed by Dr. Federico Donà (Eggert Group, King's College London). For this purpose, HeLa cells stably expressing Cas9 upon doxycycline induction (Obtained from Cheeseman Group, MIT) were transfected with GPC5 sg2 lentiGuide-Puro (Addgene #52963) and GPC5 sg3 lentiGuide-Puro. After 48 hours of transduction, the cells were selected with 2 μg/mL Puromycin.

3.7 RT-qPCR

Cells were seeded onto 6-well plates. After desired treatments have been performed, cells were scraped from the bottom of the wells and pelleted by centrifuging at 1000 rpm for 5 minutes. RNA extractions were performed using RNeasy Mini Kit (74104, QIAGEN) according to manufacturer's instructions. RT-qPCR samples were prepared using Brilliant II SYBR® Green QRT-PCR Master Mix Kit (600825, Aligent Technologies) following manufacturer's instructions and examined via ViiA 7 Real-Time PCR System (Thermo Fisher Scientific).

3.8 HRP-Based Proximity-Dependent Biotinylation and Affinity Capture of Biotinylated Proteins

HEK293T cells were grown on 150 mm dishes until they have reached 50-60% confluency. Before transfection, the media had been changed to transfection enhancement media (DMEM with 1% FBS, no antibiotics). 40 ug cMyc-HRP-GPC5 in pLenti CMV Hygro DEST and 40 ug HA-HRP-GPC3 in pLenti CMV Hygro DEST were mixed separately in 1 ml Opti-MEM in a test tube. 120 ul of PEI (1mg/ml) were added to the diluted DNA. The tubes were mixed immediately by vortexing. Mixtures were incubated at room temperature for 20 minutes. DNA/PEI mixture were added onto the cells dropwise (20 ug DNA per plate). Cell were incubated overnight in a 37˚C incubator buffered with 5% CO2. Transfection enhancement media were changed into complete DMEM (10% FBS, 1% P/S) the next day. The cells were then incubated in standard growth conditions.

After 48 hours, one plate of cMyc-HRP-GPC5 transfected HEK293T cells and one plate of HA-HRP-GPC3 transfected HEK293T cells were labelled as incubated in 15 ml complete media supplemented with 500 uM Biotin-Thyramide (LS-3500.1000, Iris Biotech GMBH)) and 1mM H_2O_2 at room temperature for 1 minute. Labelling solution were aspirated quickly after 1-minute incubation and washed three times with quencher solution containing 10mM Sodium L-Ascorbate (11140, Sigma Aldrich), 5 mM Trolox (6-hydroxy-2,5,7,8-tetramethylchroman-2-carboxylic acid,) (238813, Sigma Aldrich) and 10mM Sodium Azide (BP9221, Fisher Scientific) in PBS. Similarly, the other two plates (control plates) were incubated in 15 ml complete media supplemented with 1mM H_2O_2 only at room temperature for 1 minute and were washed quickly three times with quencher solution. 5 ml quencher solution were used to scrape the cells from the bottom of the plates. The cells were collected into falcon tubes and pelleted by centrifugation for 5 minutes at 1000 rpm at 4˚C. Supernatants were removed and the cells were kept on ice for lysis.

Cells were resuspended in 125 µl RIPA lysis buffer supplemented with 100X Protease Inhibitor and quenchers. Lysates were collected and protein concentrations were measured using Pierce™ 660nm Protein Assay Kit following manufacturer's instructions. 1 mg of lysates were loaded onto 150 µl aliquots of streptavidin beads (Pierce Streptavidin UltraLink Resin, 53117) prewashed twice with 1 ml RIPA lysis buffer and equilibrated to room temperature. The samples were incubated at 4°C overnight on a rotator.

The next day, the beads were pelleted by centrifugation (1000 rpm for 5 minutes) and supernatants. Beads were washed twice with RIPA lysis buffer, once with 1 M KCl, once with 0.1 M Na_2CO_3, once with 2 M urea in 10 mM Tris-HCl (pH 8.0), and twice with RIPA lysis buffer. 15 ul of beads were collected for Western Blot analysis.

3.9 Proteomic Profiling of Proximity Interaction Partners of GPC3 and GPC5

To identify biotinylated proteins by LC-MS/MS analyses, streptavidin beads incubated with biotinylated whole cell lysate were washed twice with 100 mM Tris-HCl (pH 8.5), twice with 8 M Urea in 100 mM Tris-HCl (pH 8.5) (Urea solution). The beads were shaken in Urea solution supplemented with 100 mM DTT at 1000 rpm for 30 minutes at 56˚C and washed with Urea solution. Then, the beads were shaken in 50 mM chloroacetamide in Urea solution at 1000 rpm for 20 minutes at 25˚C. Samples were

washed twice in Urea solution and twice in Ammonium Bicarbonate (ABC) solution (50 mM NH_4HCO_3 in HPCL water). For on-bead digestion, trypsin (Pierce™ Trypsin Protease, MS Grade, PI-90057) in 1 mM HCl was diluted 1:150 (Trypsin:WCL) and added onto beads. After 10 minutes incubation on ice, 500 µl ABC solution was added, and beads were shaken overnight at 1000 rpm at 37˚C.

The next day, beads were centrifuged at 1000 rpm for 5 minutes, and the supernatants (peptides) were collected to a fresh tube. 10% formic acid was added onto beads until reaching 1% final concentration and pH 2-3. The samples were rotated in a speed vacuum until no liquid left.

To purify the samples, C18 Stage tips were used. To condition the stage tips, 60 µl methanol and 60 µl Stage Buffer A was loaded and spined at 2500 rpm for 10 minutes, respectively. Peptides were resuspended in 60 µl Stage Buffer A (0.5% Formic Acid in 5% ACN) and sonicated for complete dissolution for 2 minutes then loaded onto stage tips and spined at 2500 rpm until all the samples flow through the stage tips (10-20 minutes). Flow through was discharged, washed with 60 µl Stage Buffer A, and spined at 2500 rpm for 10 minutes. Tips were placed on clean 1.5 ml tubes and peptides were eluted by adding 60 µl Stage Buffer B (0.1% Formic Acid in 70% ACN) and spinning at 3000 rpm for 15 minutes. The samples were dried in speed vacuum until no liquid left.

Peptides were analysed by on-line C18 nanoflow reversed-phase HPLC linked to a Q-Exactive Orbitrap mass spectrometer (Thermo Scientific). The data sets were searched against the human Uniprot database. Thermo Discoverer 2.3 software was used to identify proteins. The STRING v.11 database was used to reveal network maps of interactomes and gProfiler version e101_eg48_p14_baf17f0 has been used for GO cellular component analyses of the final protein lists. The protein interaction network was visualized using Cytoscape 3.8.2.

** The preliminary analysis of the protein lists was performed by **Altuğ Kamacıoğlu**.*

3.10 Western Blotting and Immunostaining

For western blotting, samples were separated using 8%, 10%, and 12% SDS-PAGE under reducing conditions depending on the molecular weights of proteins to be investigated. Transfer of proteins to nitrocellulose membranes were carried out by

BioRad wet transfer system either by permorming a 2 hours transfer at 100V at room temperature, or an overnight transfer at 35V at 4˚C.After transfer, membranes were blocked by 4% Non-Fat Milk in TBS-1% Tween-20 (TBS-T) for 1 hour at room temperature with gentle shaking.. After blocking membranes were incubated with desired primary antibodies either for 3 hours at room temperature or overnight at +4˚C. After primary antibody incubation, membranes were washed 3 times in TBS-T for 5 minutes. Then, HRP-Conjugated secondary antibodies were used for ECL(Thermo Scientific, 32132) detection. Blots were imaged by using either X-ray films or Chemidoc (BioRad). The primary and secondary antibodies used for Western Blotting are listed on Table 3.1.

Table 3. 1: Western blotting antibodies and dilutions.

Antibody	Host	Dilution Factor	Company	Product Number
Anti-Biotin	Rabbit	1:20000	Noncommercial	Noncommercial
Anti-myc	Rabbit	1:1000	Cell Signaling	71D10
HA-probe	Rabbit	1:500	Santa Cruz	SC-805
Anti-Rabbit IgG-HRP	Goat	1:2000	Cell Signaling	7074S
Anti-Mouse IgG-HRP	Horse	1:2000	Cell Signaling	7076S

For immunostaining, cells were seeded onto 18 mm coverslips. After appropriate treatments were performed, cells were fixed using 4% paraformaldehyde for 15 minutes at 37˚C. Samples were blocked by 2% BSA in 0.1% Triton-X PBS for 1 hour at room temperature. Then, samples were incubated in primary antibodies diluted in 2% BSA in 0.1% Triton-X PBS either for 3 hours at room temperature or overnight at +4˚C. Samples were washed 3 times with 0.1% Triton-X PBS for 5 minutes. Then, samples were incubated with secondary antibodies and DAPI diluted in 2% BSA in 0.1% Triton-X PBS for 1 hour at room temperature. Samples were washed again 3 times with 0.1% Triton-X PBS and 1 last time in PBS. Coverslips were finally mounted in mowiol mounting medium. The primary and secondary antibodies used for immunostaining are listed on Table 3.2.

Table 3. 2: Immunostaining antibodies and dilutions.

Antibody	Host	Dilution Factor	Company	Product Number
Anti-Tubulin	Mouse	1:400	Sigma	T9026
Anti-myc	Rabbit	1:400	Cell Signaling	71D10
Anti-HA	Mouse	1:1000	BioLegend	B291379
Anti-Phospho-Myosin Light Chain (Ser19)	Mouse	1:100	Cell Signaling	3675S
Anti-Ezrin	Rabbit	1:200	Cell Signaling	3145S
Anti-P-ERM (T567)	Rabbit	1:100	Cell Signaling	3726S
Anti-Anillin	Rabbit	1:400	Abcam	Ab99352
Anti-Alix (PDC6I)	Rabbit	1:500	Abcam	Ab88388
Streptavidin Alexa Flour 488	-	1:2000	Life Technologies	1316703
Phalloidin-iFlour	-	1:5000	Abcam	Ab176756
Anti-mouse IgG Alexa Flour (H+L) 488	Donkey	1:1000	Life Technologies	A21202
Anti-Rabbit IgG (H+L) Dylight 488	Goat	1:1000	Thermo Scientific	35552
Anti-rabbit IgG Alexa Flour 555 Fab2	Goat	1:1000	Cell Signaling	4413S
Anti-mouse IgG Alexa Flour (R) 555 Fab2	Goat	1:1000	Cell Signaling	4409S

3.11 Microscopy and Quantification

Live cell fluorescent and bright field imaging were acquired with Leica DMi8 widefield microscope equipped with HC PL APO 63x/1.40-0.60 OIL objective. Fixed samples were imaged by Leica DMi8/SP8 TCS-DLS laser scanning confocal microscope, Nikon A1 HD25 confocal microscope and Leica DMi8 widefield microscope. Quantifications of images were performed by FIJI (ImageJ) software. Statistical analyses were performed by GraphPad Prism 8 Software.

Chapter 4:

RESULTS

4.1 GPC3 And GPC5 Enrich at The Cleavage Furrow During Cytokinesis

To understand the spatiotemporal regulation of GPC3 and GPC5 in cell division, EGFP-tagged constructs were created by Gibson assembly. HeLa Kyoto cells were transfected with these constructs and visualized by live cell imaging.

At metaphase and anaphase, GPC3 (**Figure 4.1**) and GPC5 (**Figure 4.2**) localize on the cell membrane, with no observable enrichment on any part on the membrane. At early telophase stage both GPC3 and GPC5 slightly enriches at the cleavage furrow. At mid telophase, enrichment at the cleavage furrow increases for both proteins and peaks at late telophase.

Quantifications of GFP-GPC3 (**Figure 4.1**) and GFP-GPC5 (**Figure 4.2**) signals at the cleavage furrow at mid telophase, using myr-PALM-GFP transfected HeLa Kyoto cells as controls, have showed a significant increase. Therefore, we concluded that GPC3 and GPC5 enrich at the cleavage furrow during cytokinesis.

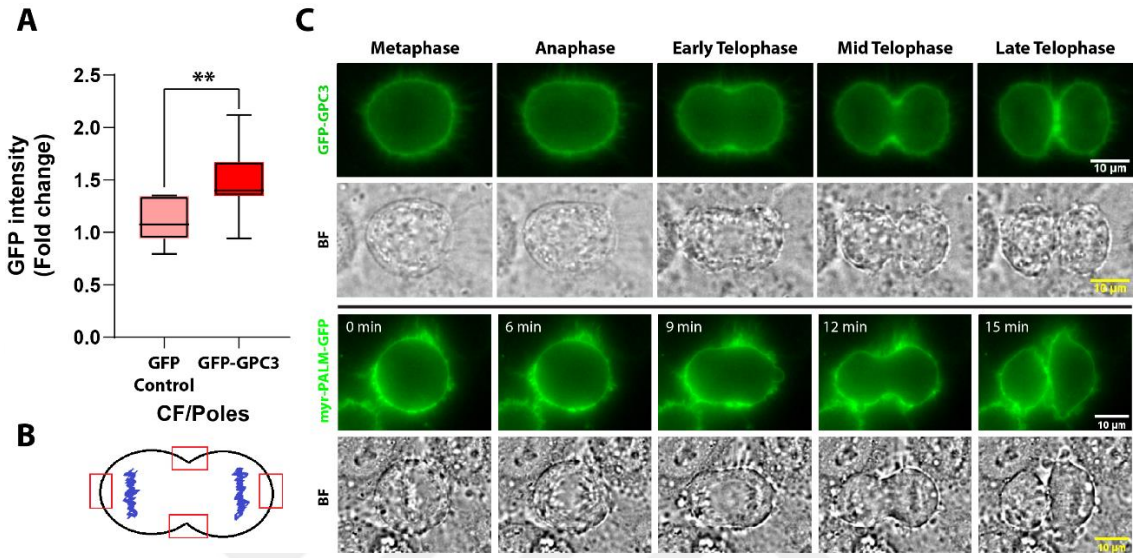

Figure 4. 1: GPC3 enriches at the cleavage furrow during cytokinesis.

A) Quantification of GFP intensities at mid telophase stage. Average GFP intensities at the cleavage furrow were divided by the average intensities at cell poles for each cell. Data presented as n= 7 for control and n=15 for GFP-GPC3. Unpaired two-tailed Student's t test has been used for significance analysis, **: p=0.0061. **B)** A scheme illustrating the areas analyzed (cleavage furrow and cell poles) for quantification on part A. **C)** Representative images of GFP-GPC3 (upper panel) and myr-PALM-GFP (lower panel) expressing HeLa Kyoto cells at different mitotic stages. Scale bars 10 µm.

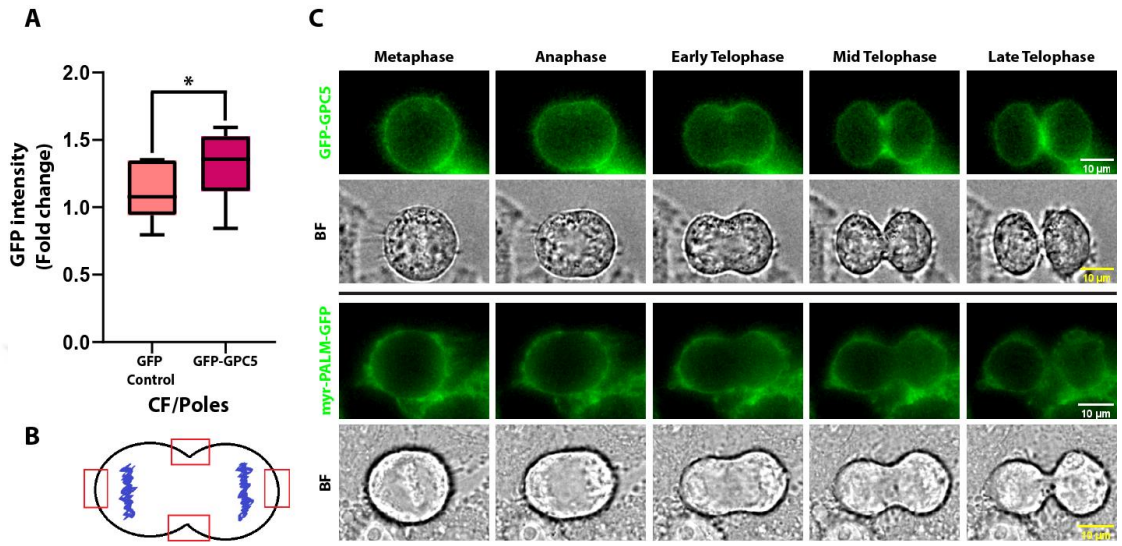

Figure 4. 2: GPC5 enriches at the cleavage furrow during cytokinesis.

A) Quantification of GFP intensities at mid telophase stage. Average GFP intensities at the cleavage furrow were divided by the average intensities at cell poles for each cell. Data presented as n= 7 for control and n=12 for GFP-GPC5. Unpaired two-tailed Student's t test has been used for significance analysis, *: p=0.0449. **B)** A scheme illustrating the areas analyzed (cleavage furrow and cell poles) for quantification on part A. **C)** Representative images of GFP-GPC3 (upper panel) and myr-PALM-GFP (lower panel) expressing HeLa Kyoto cells at different mitotic stages. Scale bars 10 µm..

4.2 Knocking Out GPC5 Causes Defects in Cell Division

After showing that GPC3 and GPC5 enrich at the cleavage furrow after cytokinesis, we wanted to investigate if GPC5 knock out causes cell division defects. To this end, we obtained inducible CRISPR/Cas9 HeLa cells (HeLaCas9 cells) and single-guide RNA vectors targeting GPC5 from Eggert Group, King's College London. (sgRNAs were designed by Dr. Federico Dona.) sgRNA vectors were stably expressed at HeLaCas9 cells by virus transduction. (HeLaCas9 GPC5 sg1.8 cells were previously created by Dr. Federico Dona from Eggert Group, King's College London.)

I created HeLaCas9 GPC5 sg2 cell line as a biological replicate of HeLaCas9 GPC5 sg1.8. Upon 72-hour Dox induction, GPC5 knock out efficiencies of both sg1.8 and sg2 expressing HeLaCas9 cells were determined by qRT-PCR (**Figure 4.3**). Among those, upon Dox induction, 94% decrease in GPC5 expression has been shown in HeLaCas9 GPC5 sg1.8 cells (**Figure 4.3, left panel**), whereas 83% decrease in GPC5 expression has been detected in HeLaCas9 GPC5 sg2 cells (**Figure 4.3, right panel**).

4.2.1 Knockout of GPC5 Leads to Multinucleation

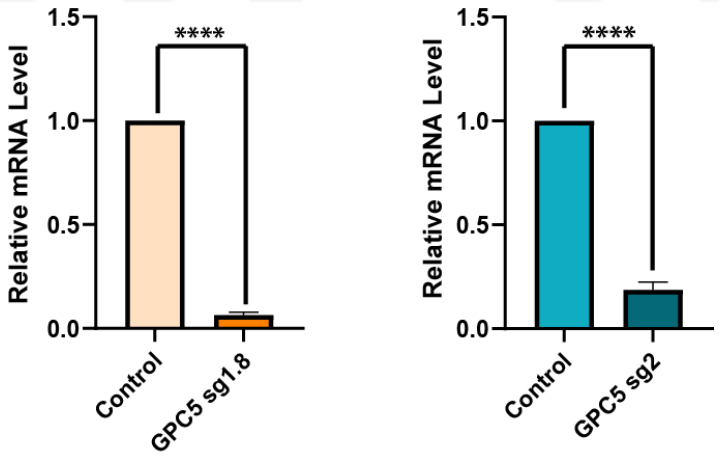

Figure 4. 3: qRT-PCR of Dox inducible GPC5 knock out cells.

Left panel: Dox induced HeLaCas9 GPC5 sg1.8 cells showed 94% decrease in GPC5 expression. Right panel: Dox induced HeLaCas9 GPC5 sg2 cells showed 83% decrease in GPC5 expression. (Error bars represent ± SEM, N=3 biological replicates, ****: $p < 0.0001$)

GPC5 knockout led to multinucleation in both cell lines. Upon 72 hours Dox induction, the percentage of binucleated HeLaCas9 GPC5 sg1.8 cells were significantly increased from 2.46% to 4.01% (**Figure 4.4**).

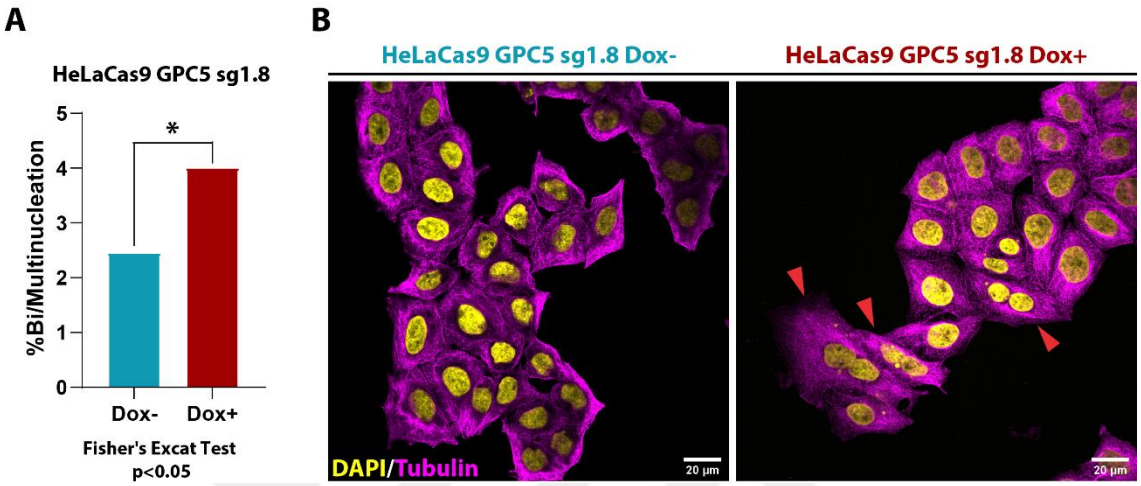

Figure 4. 4: GPC5 knock out leads to multinucleation in HeLaCas9 GPC5 sg1.8 cells.

A) Quantification of percentage of multinucleated cells in control (Dox-) and GPC5 knock out (Dox+) HeLaCas9 GPC5 sg1.8 cells. Data represented as n= 1073 for Dox+ and n=1260 for Dox-. Fisher's exact test with odds ratio has been performed for significance analysis, *: p= 0.04232. **B)** Representative images of control (left panel) and GPC5 knock out (right panel) cells. Red arrowheads show multinucleated cells. Scale bars: 20 µm.

Similarly, upon GPC5 knockout, the percentage of binucleated HeLaCas9 GPC5 sg2 cells were significantly increased from 1.39% to 6.71% (**Figure 4.5A**). Moreover, multinucleation phenotype has been rescued by ectopic expression of CRISPR-resistant cMyc-GPC5 (4.86% and 4.25%) (**Figure 4.5B**).

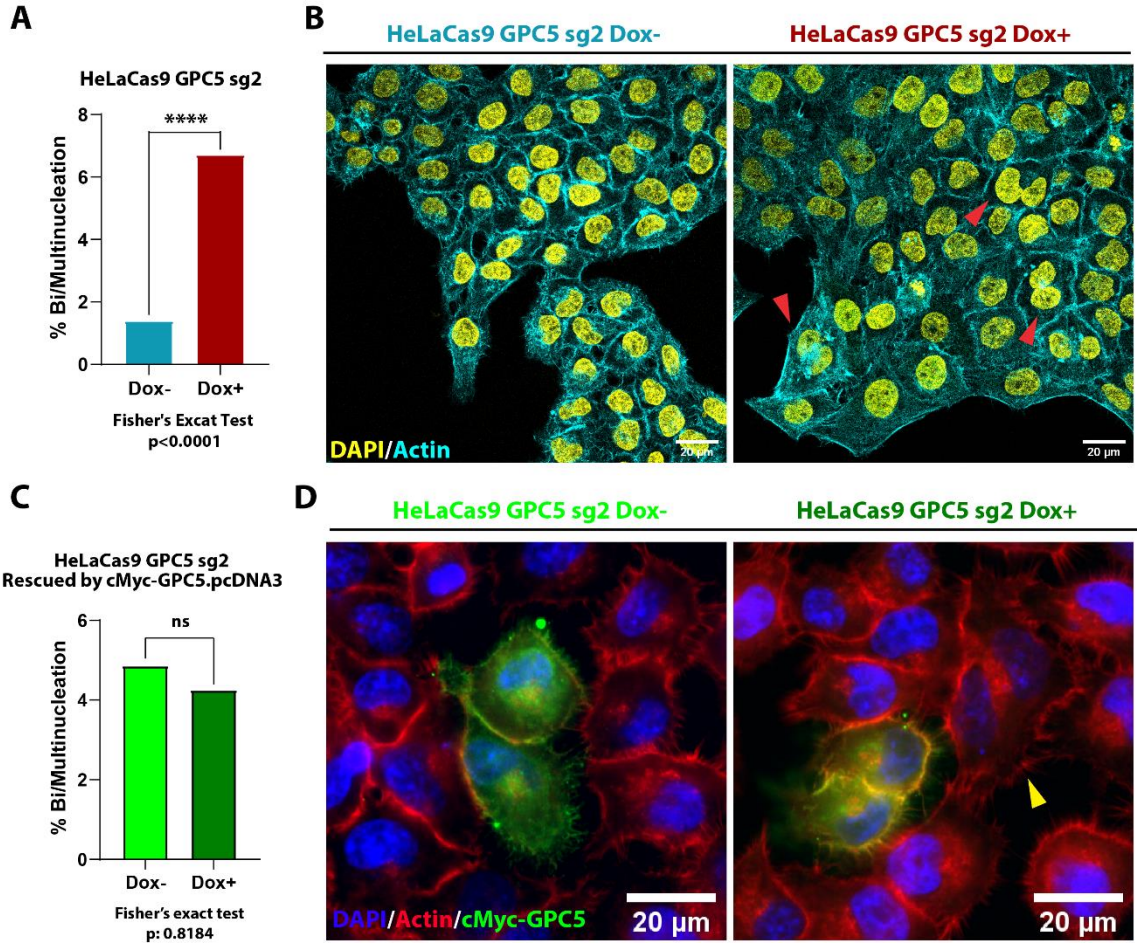

Figure 4. 5: GPC5 knock out leads to multinucleation in HeLaCas9 GPC5 sg2.

A) Quantification of the percentage of multinucleated cells in control (Dox-) and GPC5 knock out (Dox+) HeLaCas9 sg2 cells. Data represented as n= 1551 for Dox+ and n=1007 for Dox- for control and HeLaCas9 GPC5 sg2 knock out cells. Fisher's exact test with odds ratio has been performed for significance analysis, ****: $p<0.0001$. **B)** Representative images of control (left panel) and GPC5 knock out (right panel) cells. Red arrowheads show multinucleated cells. **C)** Quantification of the percentage of multinucleated cells in control (Dox-) and GPC5 knock out (Dox+) HeLaCas9 sg2 cells transfected with CRISPR-Resistant cMyc-GPC5 construct. Data represented as n=259 for Dox+ and n=185 for Dox- for cMyc-GPC5 rescue cells. Fisher's exact test with odds ratio has been performed for significance analysis, ns: not significant. **D)** Representative images of control (left panel) and GPC5 knock out (right panel) cells transfected with CRISPR-resistant cMyc-GPC5 construct. Yellow arrowhead shows a multinucleated cell. Scale bars: 20 µm.

4.2.2 GPC5 Knockout Does Not Affect the Localization of Certain Proteins Involved in Cytokinesis

To understand how GPC5 knock out causes multinucleation, we wanted to imagine the localizations of certain proteins that regulate cytokinesis. To this end, localizations of phosphorylated-Myosin (**Figure 4.6**), Ezrin and phosphorylated-Ezrin (p-ERM) (**Figure 4.7**), Anillin and Alix (**Figure 4.8**) have been examined by immunostaining in dividing cells. None of these proteins showed a significant difference in localization in GPC5 knockout cells compared to control cells.

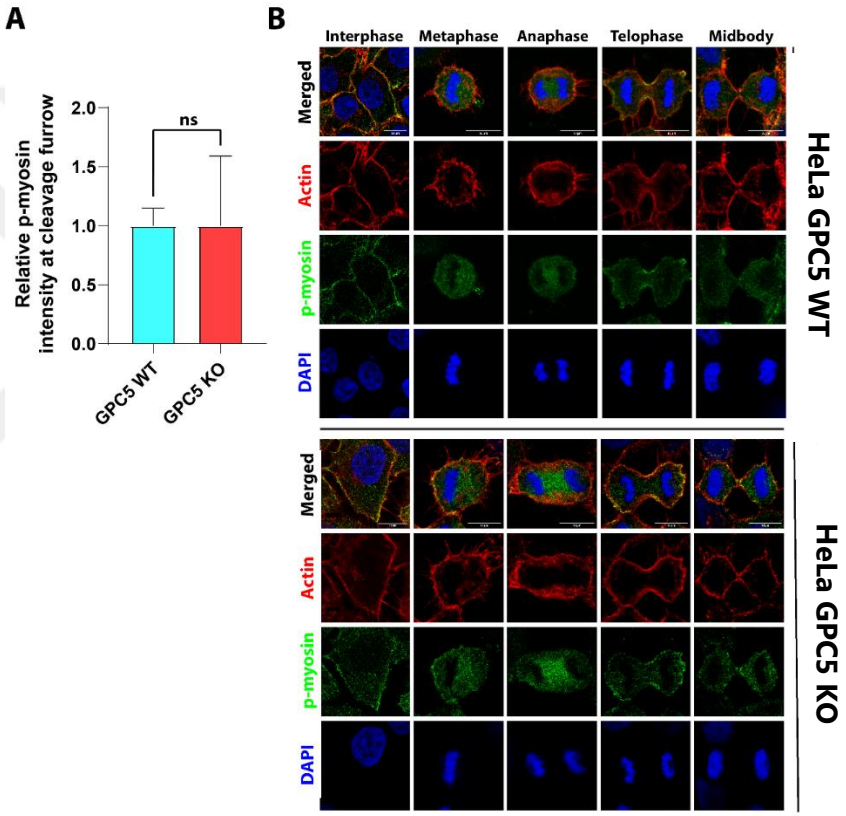

Figure 4. 6: Localization of p-myosin in control and GPC5 knock out cells.

A) Quantification of relative p-myosin intensity at cleavage furrow of control (GPC5 WT) and GPC5 knock out (GPC5 KO) cells. Data presented as n=9 for controls and n=12 for GPC5 KO cells. Unpaired two-tailed Student's t test has been performed for significance analysis, ns: not significant. **B)** Representative images of localization of p-myosin in interphase, metaphase, anaphase, telophase, and midbody of control (HeLa GPC5 WT) and GPC5 knock out (HeLa GPC5 KO) HeLaCas9 GPC5 sg2 cells. Scale bars: 10 µm.

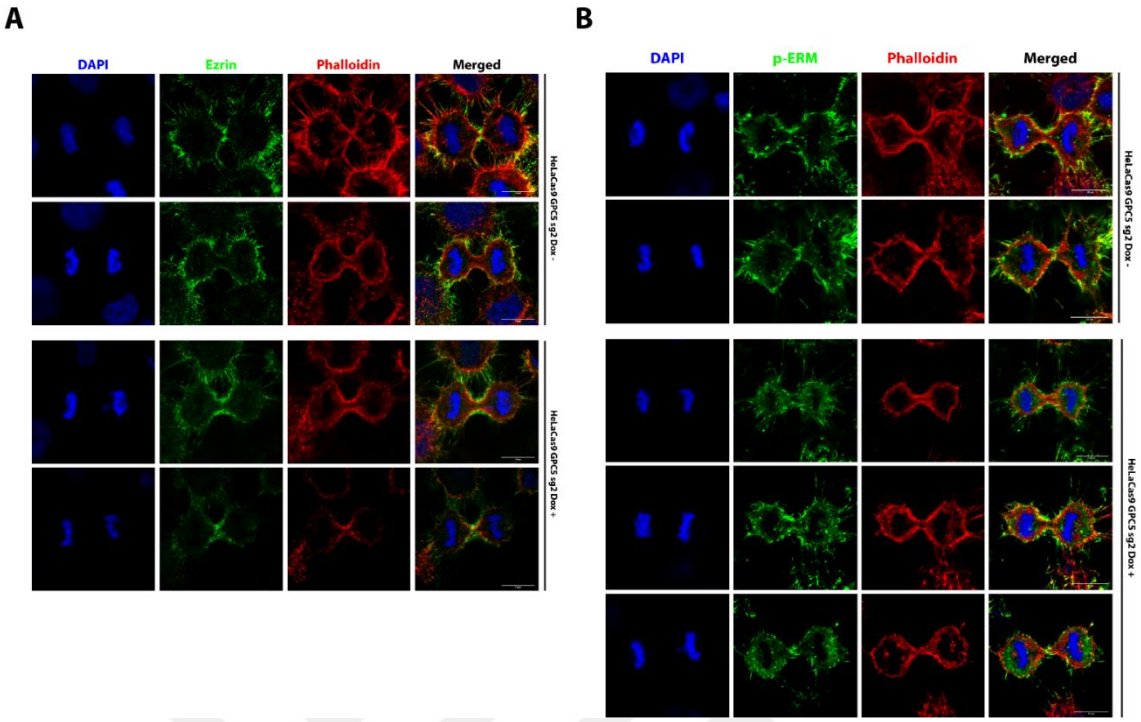

Figure 4. 7: Localization of Ezrin (A) and p-ERM (B) late telophase in control and GPC5 knock out HeLaCas9 GPC5 sg2 cells.

Scale bars: 10 µm.

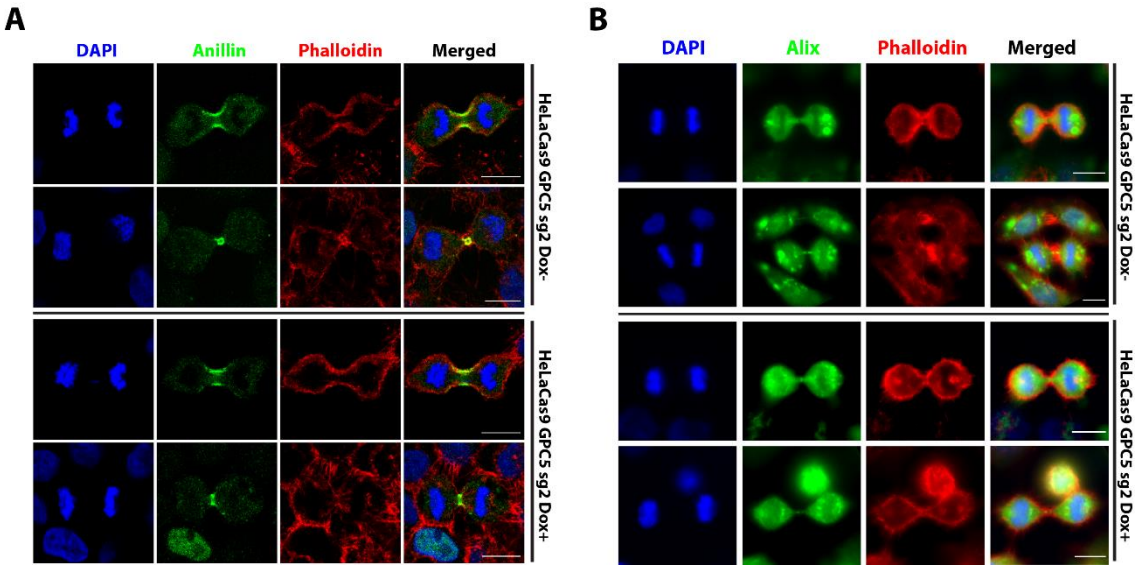

Figure 4. 8: Localization of Anillin (A) and Alix (B) late telophase in control and Dox induced HeLaCas9 GPC5 sg2 cells.

Scale bars: 10 µm.

4.2.3 GPC5 Knockout Causes Defects at Different Stages of Cell Division

To characterize the defects in GPC5 knockout cells that lead to multinucleation, we performed live cell imaging experiments of control and GPC5 knockout cells and investigated the cell division phenotypes. In all samples, GPC5 knockout cells were able to round up as control samples; however, defects at the following stages of cell division have been observed.

The first defect detected in the GPC5 knockout cells after cell rounding was chromosome jiggling. The percentage of cells exhibiting chromosome jiggling was increased from 1.79% to 11.43% in GPC5 knockout cells compared to controls. However, this increase was not statistically significant (**Figure 4.9**).

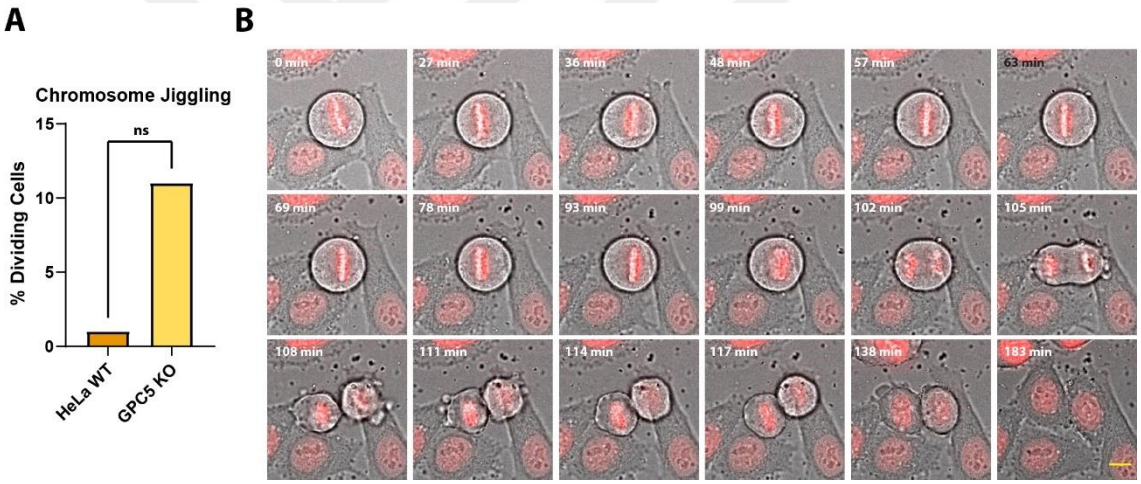

Figure 4. 9: Chromosome jiggling phenotype in dividing control and GPC5 knockout cells.

A) Quantification of the percentage of dividing cells exhibiting chromosome jiggling in control (HeLa WT) and GPC5 knock out (GPC5 KO) HeLaCas9 sg2 cells. Data presented as n=56 for controls and n=35 for GPC5 knockout cells. Fischer's Exact Test has been performed for significance analysis. ns: not significant, p=0.07. **B)** Merged live cell fluorescent and bright field imaging of H2B-mCherry expressing Dox induced HeLaCas9 GPC5 sg2 cells. Scale bar: 10 µm.

Another defect identified in the GPC5 knockout cells in cell division was shifted division plane. While the contractile rings of the control cells are formed perpendicular to the attachment surface with only 1.8% of them exhibiting abnormal division plane orientation, 29.7% of GPC5 knockout cells exhibit defective division plane orientation (**Figure 4.10**). These defective cells form angular contractile rings toward the attachment surface. Moreover, in some cases, the contractile rings of the GPC5 knockout cells are formed reciprocal to the attachment surface. This phenomenon is illustrated in **Figure 4.11**.

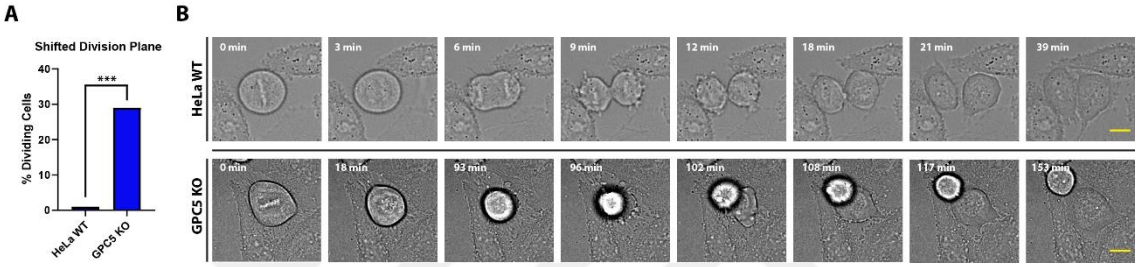

Figure 4. 10: Shifted division plane phenotype in dividing control and GPC5 knockout cells.

A) Quantification of the percentage of dividing cells exhibiting shifted division plane in control (HeLa WT) and GPC5 knock out (GPC5 KO) HeLaCas9 sg2 cells. Data presented as n=56 for controls and n=37 for GPC5 knockout cells. Fischer's Exact Test has been performed for significance analysis. ***: p=0.0001. **B)** Live cell bright field imaging of control (HeLa WT - upper panel) and Dox induced HeLaCas9 GPC5 sg2 (GPC5 KO – lower panel) cells. Scale bar: 10 µm.

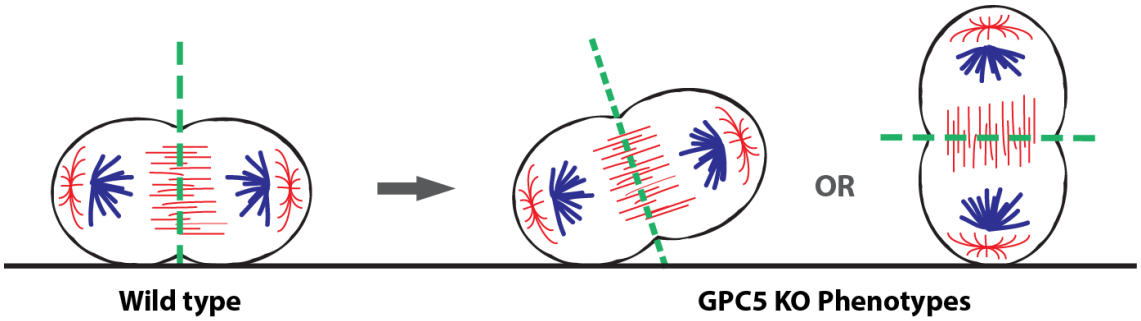

Figure 4. 11: Illustration of shifted division plane phenotype of control and GPC5 knockout cells.

Blue lines represent chromosomes, red lines represent astral and spindle microtubules.

GPC5 knockout cells also showed increased membrane blebbing at cleavage furrow. While 12.5% of the control cells exhibited cleavage furrow blebbing, this phenotype is observed in 30% of GPC5 knockout cells (**Figure 4.12**). Maximal lengths of cleavage furrow blebs of GPC5 knockout cells are significantly increased compared to control cells. The median of bleb lengths at the cleavage furrows of control cells is 3.245 µm whereas the median of the length of cleavage furrow blebs of GPC5 knockout cells is be 5.680 µm (**Figure 4.13**).

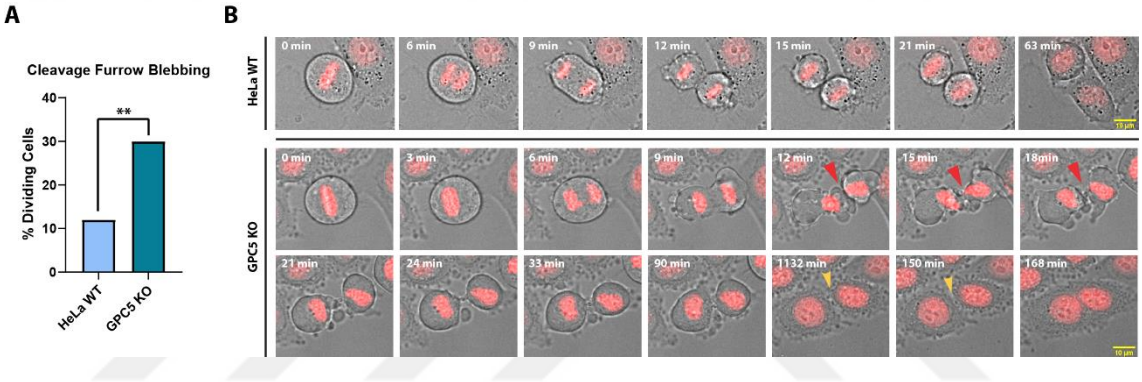

Figure 4. 12: Cleavage furrow blebbing phenotype in dividing control and GPC5 knockout cells expressing H2B-mCherry.

A) Quantification of the percentage of dividing cells exhibiting cleavage furrow blebbing in control (HeLa WT) and GPC5 knock out (GPC5 KO) H2B-mCherry expressing HeLaCas9 sg2 cells. Data presented as n=88 for control cells and n=100 for GPC5 knockout cells. Fischer's Exact Test has been performed for significance analysis, **: p=0.0045. **B)** Merged lice cell fluorescent and bright field imaging of H2B-mCherry expressing control (HeLa WT - upper panel) and Dox induced HeLaCas9 GPC5 sg2 (GPC5 KO – lower panel) cells. Red arrowheads indicate cleavage furrow blebbing, yellow arrowheads indicate midbody. Scale bars: 10 µm.

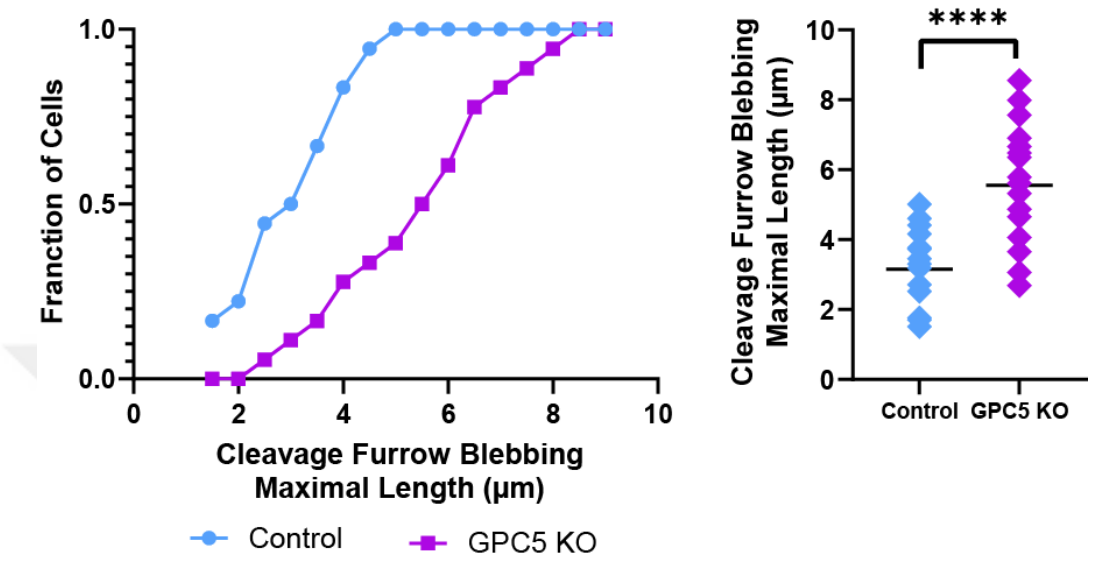

Figure 4. 13: Quantification of maximal length of cleavage furrow blebbing in control and GPC5 knockout cells.

Data presented as n=18 for both control and GPC5 knockout cells. Unpaired two-tailed Student's t test has been performed for significance analysis. Black lines in the right graph show mean length. ****: $p<0.0001$.

Similar to the cleavage furrow blebbing phenotype, the maximum length of blebs at the cell poles were also significantly increased in GPC5 knockout cells compared to controls (**Figure 4.14**). While the median of the length of polar blebs of the control cells is 3.235 µm, it is 5.430 µm for GPC5 knockout cells (**Figure 4.15**).

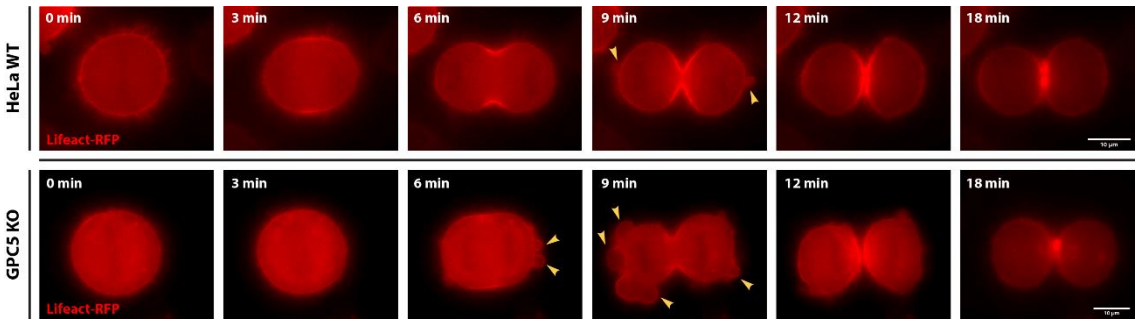

Figure 4. 14: Polar blebbing phenotype in dividing control and GPC5 knockout cells expressing Lifeact-RFP.

Live cell fluorescent imaging of Lifeact-RFP expressing control (HeLa WT - upper panel) and Dox induced HeLaCas9 GPC5 sg2 (GPC5 KO – lower panel) cells. Yellow arrowheads indicate polar blebbing. Scale bars: 10 µm.

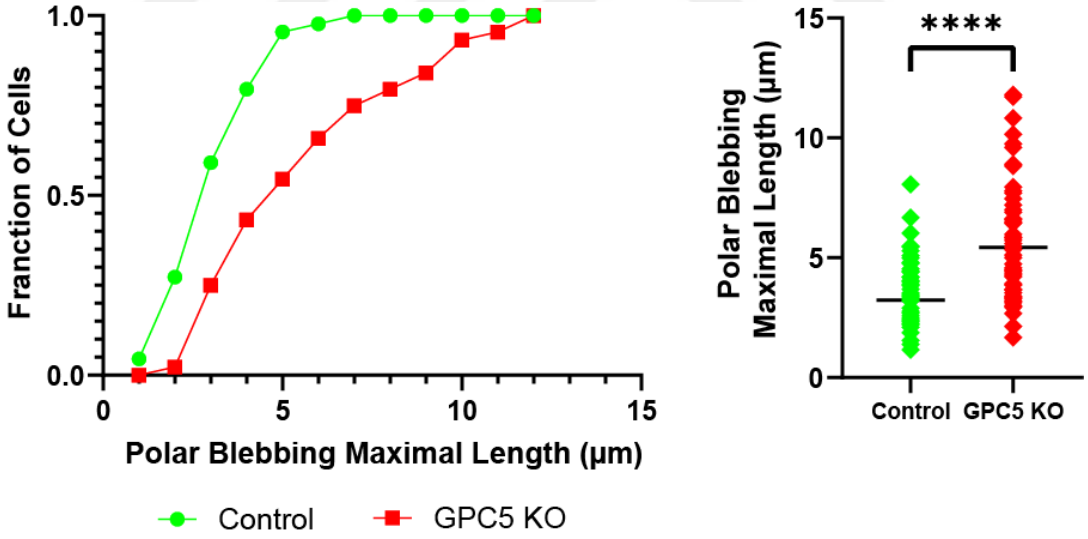

Figure 4. 15: Quantification of maximal length of polar blebbing in control and GPC5 knockout cells.

Data presented as n=60 for both control and GPC5 knockout cells. Unpaired two-tailed Student's t test has been performed for significance analysis. Black lines in the right graph show mean length. ****: $p<0.0001$.

Lastly, as indicated before in this section, GPC5 knockout cells exhibit significantly increased number of multinucleated cells compared to control samples. Initial observations showed that multinucleation occurs after incomplete midbody abscission followed by regression of the cleavage furrow (Figure 4.16). In addition, GPC5 knockout cells exhibited significantly prolonged midbody abscission time compared to control cells (Figure 4.17).

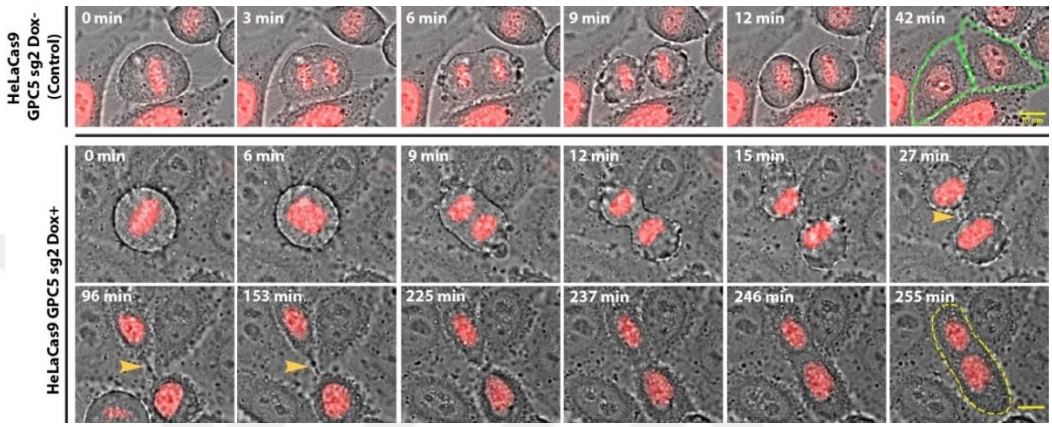

Figure 4. 16: Live cell fluorescent and bright field imaging of control and GPC5 knockout cells expressing H2B-mCherry.

Merged lice cell fluorescent and bright field imaging of H2B-mCherry expressing control (upper panel) and Dox induced HeLaCas9 GPC5 sg2 (lower panel) cells. Yellow arrowheads indicate midbody. Successfully divided daughter cells are marked with green dashed lines. Binucleated cell is marked with yellow dashed lines. Scale bars: 10 µm.

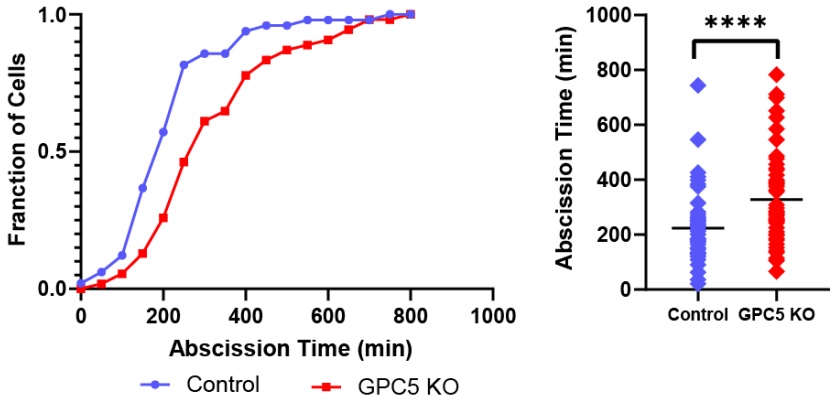

Figure 4. 17: Quantification of abscission time of control and GPC5 knockout cells.

Data presented as n=54 for both control and GPC5 knockout cells. Unpaired Student's t test has been performed for significance analysis. Black lines in the right graph show mean length. ****: $p<0.0001$.

4.3 Identification of the Interaction Partners of GPC3 and GPC5

To understand the roles of GPC3 and GPC5 in cytokinesis and further investigate the underlying factors of the defects in the cell division of GPC5 knockout cells, we aimed to identify the interaction partners of GPC3 and GPC5 by HRP-based proximity labeling followed by LC-MS/MS analysis.

In order to perform HRP-based proximity labeling, we first created HRP-tagged GPC3 and GPC5 constructs. Since both *gpc3* and *gpc5* genes contain signal sequences in their N-termini and GPI-binding site in their C-termini [16], we inserted HRP sequence in between cMyc (or HA) and core protein sequence by Gibson assembly. An illustration of the insertion site and the resulting proteins is shown below in **Figure 4.18**.

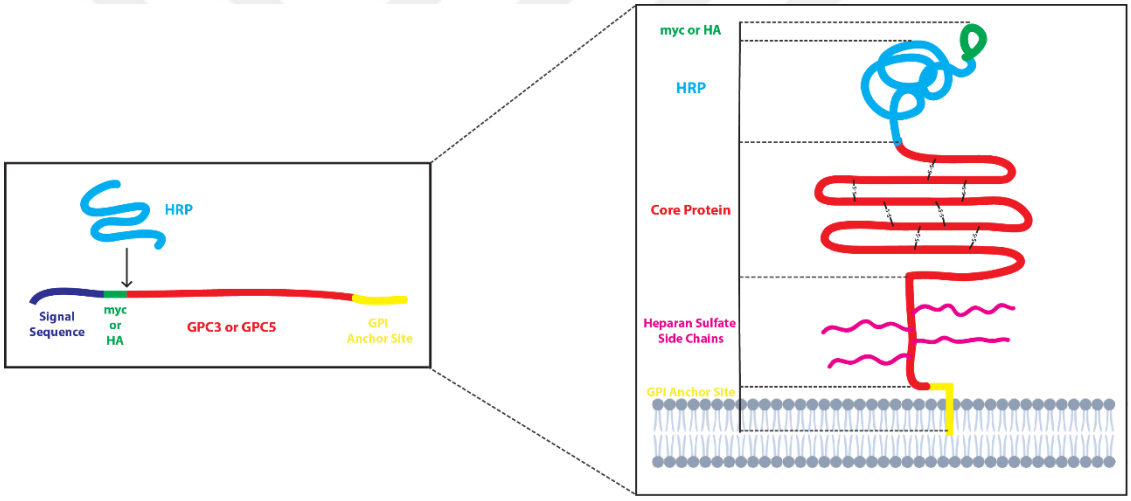

Figure 4. 18: Illustration of HRP insertion site and resulting proteins of HRP-tagged GPC3 and GPC5 constructs.

After the HRP-tagged GPC3 and GPC5 constructs were created and sequenced, we performed HRP-based proximity labelling and identified the interaction partners of GPC3 and GPC5 in asynchronous HEK293T cells as well as HEK293T cells synchronized to monopolar cytokinesis.

4.3.1 HRP-Based Proximity Labelling

After creating HRP-tagged GPC3 and GPC5 constructs, HRP-based proximity labelling was first performed in HeLa Kyoto cells transfected with myc-HRP-GPC5 and HA-HRP-GPC3 constructs to ensure that the system works successfully. Firstly, successful cell surface biotinylation was confirmed with immunostaining. As shown in **Figure 4.19**, transfected cells showed cell surface biotinylation in the presence of both Biotin-Phenol (BP) and hydrogen peroxide (H_2O_2) whereas no cell surface biotinylation was observed in samples treated with only H2O2 or samples receiving no treatment. Biotinylation in multiple proteins has also been shown by Western blotting where only endogenously biotinylated proteins has been observed in transfected samples treated with either only BP or only H_2O_2 (**Figure 4.20**).

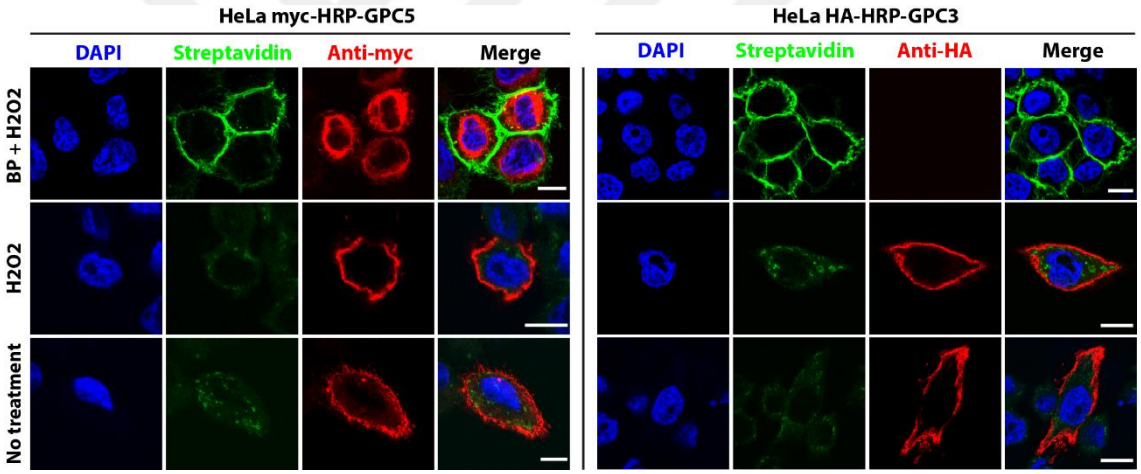

Figure 4. 19: Representative microscopy images of HeLa cells expressing cMyc-HRP-GPC5 (left) and HA-HRP::GPC3 (right).

Biotin, DNA and Myc-HRP\HA-HRP fusion proteins were labelled with Streptavidin (green), DAPI (blue) and anti-myc/anti-HA antibodies (red), respectively. Cell surface biotinylation was only observed in BP+H2O2 experimental condition (top) but not in the negative controls (middle, bottom). Scale bars: 10 µm.

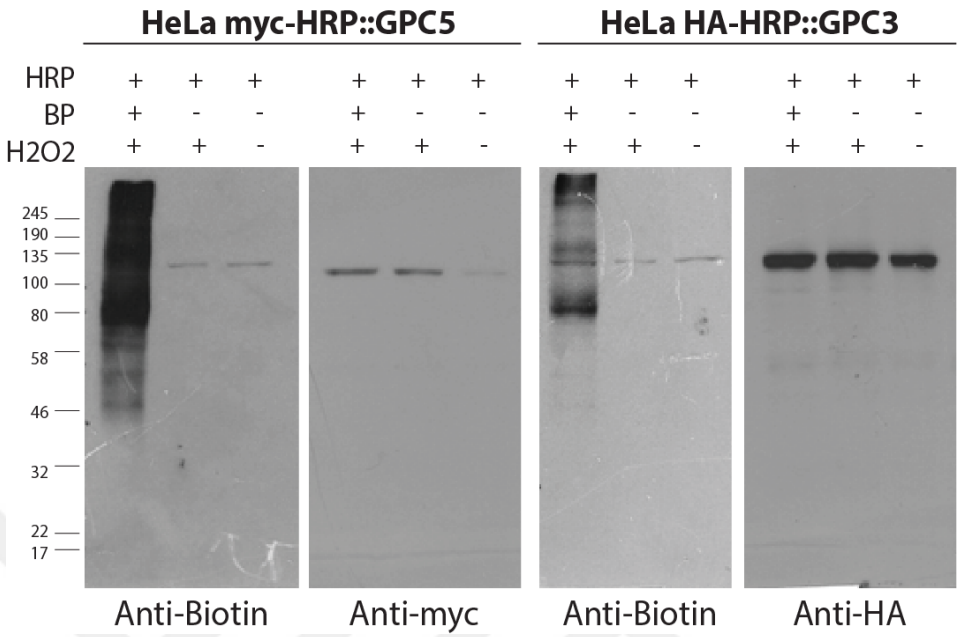

Figure 4. 20: Western blotting analysis of HeLa cells expressing cMyc-HRP::GPC5 (left) and HA-HRP::GPC3 (right).

Biotinylation at multiple proteins were observed in cMyc-HRP::GPC5 and HA-HRP::GCP3 expressing cells incubated with BP (Biotin-Phenol) and H_2O_2 but not in negative controls.

After successful cell surface biotinylation in multiple cell surface proteins in cells transfected with HRP-tagged GPC3 and GPC5 constructs has been confirmed, we wanted to confirm that streptavidin enrichment is sufficient. To this end, after incubating the lysates of biotinylated and control samples on Streptavidin beads, washing the beads with appropriate buffers, and eluting a small fraction of beads as described in Materials and Methods section, Western blot analysis was performed. The samples were blotted with anti-Biotin antibody and imaged. Western blotting revealed that biotinylated proteins were successfully enriched by streptavidin beads (**Figure 4.21**).

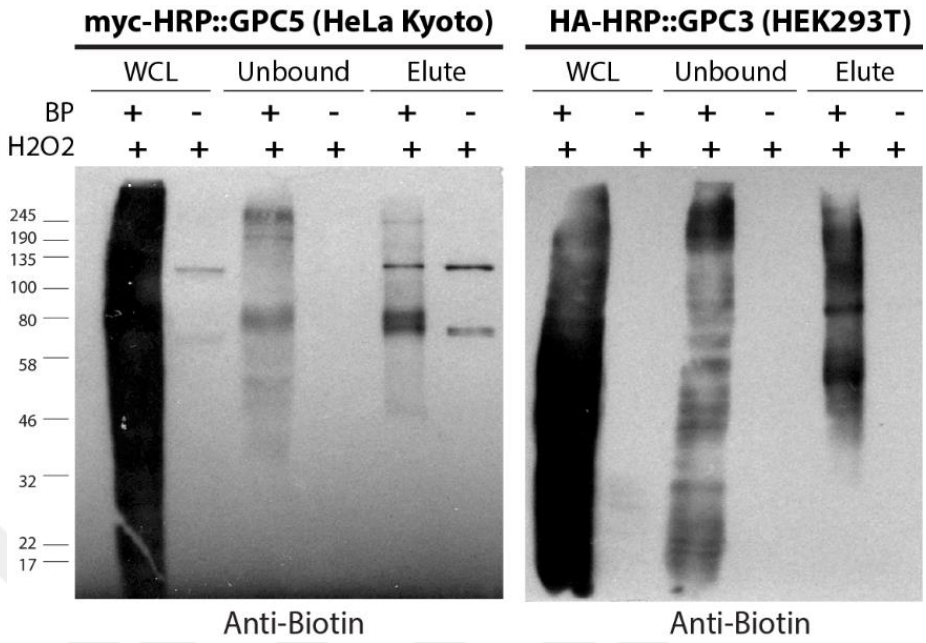

Figure 4. 21: Western blotting analysis of Streptavidin enrichment of HeLa Kyoto and HEK293T cells transfected with myc-HRP-GPC5 (left) and HA-HRP-GPC3 (right panel) constructs, respectively.

Pulldown of biotinylated proteins has been shown in elutes in the cells incubated with BP and H2O2. The lines in the samples that were only treated with H2O2 in the left panel show endogenously biotinylated proteins. WCL: Whole Cell Lysate.

After the confirmation steps described above, on-bead trypsin digestions were performed to identify the interaction partners of GPC3 and GPC5 by LC-MS/MS analysis. *Table 4.1* shows the details of samples analyzed by LC-MS/MS.

Table 4. 1: Samples analyzed by LC-MS/MS.

Cell line	**Transfected with:**	**Synchronization:**	**Number of Biological Replicates:**	**Bait coverages:**
HEK293T	cMyc-HRP-GPC5	Interphase (Asynchronous)	2	15% and 12%
HEK293T	cMyc-HRP-GPC5	Cytokinesis (Synchronized)	3	10%, 9%, and 10%
HEK293T	HA-HRP-GPC3	Interphase (Asynchronous)	1	23%
HEK293T	HA-HRP-GPC3	Cytokinesis (Synchronized)	3	22%, 17%, and 6%

The LC-MS/MS analyses specified in *Table 4.1* has been analyzed by SAINT software. The number of significantly enriched proteins identified in SAINT analysis is detailed in *Table 4.2* below.

Table 4. 2: Numbers of significantly enriched proteins identified by SAINT analysis.

Cell line	**Transfected with:**	**Cell Cycle Stage**	**Significantly enriched proteins identified in SAINT analysis:**
HEK293T	cMyc-HRP-GPC5	Interphase (Asynchronous)	119
HEK293T	cMyc-HRP-GPC5	Cytokinesis (Synchronized)	38
HEK293T	HA-HRP-GPC3	Interphase (Asynchronous)	635
HEK293T	HA-HRP-GPC3	Cytokinesis (Synchronized)	22

4.3.2 Interaction Partners of GPC5

By applying HRP-based proximity labeling, we identified 119 proteins in interphase cells as GPC5 interactors. In HEK293T cells synchronized to monopolar cytokinesis, we performed SAINT analysis only to those samples where GPC5 coverages were equal to or greater than 10%. In these analyses, 38 proteins were identified as GPC5 interactors: 22 of these proteins were common in interphase and cytokinesis in HEK293T cells. A Venn diagram summarizing the distribution of GPC5 interactors among asynchronous and synchronized HEK293T cells is shown in **Figure 4.22**.

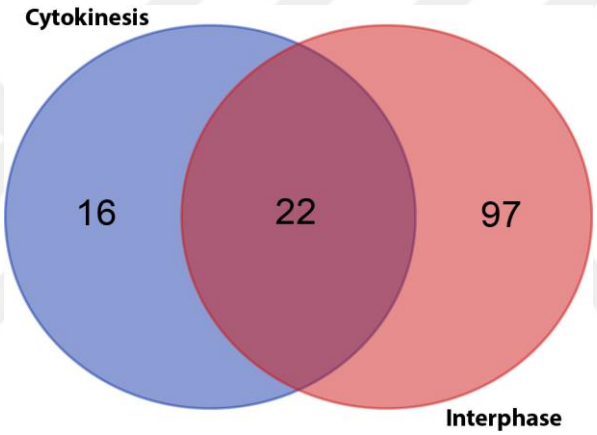

Figure 4. 22: Venn diagram showing the common GPC5 interactors in HEK293T cells.

Cellular localizations and functions of interaction partners of GPC5 during cytokinesis is listed in *Table 4.3*. Localizations and molecular functions of these proteins have been retrieved from UniProt database. In addition, network clustering of GPC5 interactors during cytokinesis is illustrated in **Figure 4.23** and network clustering of GPC5 interactors at interphase is illustrated in **Figure 4.24**.

Table 4. 3: Cellular localizations and functions of interaction partners of GPC5 during cytokinesis.

Gene Name	Protein Name	Cellular Localization	Function
GPC5	**Glypican 5**		
ALCAM	**CD166 antigen**	Plasma membrane	Cell adhesion
SLC3A2	**4F2 cell-surface antigen heavy chain**	Plasma membrane	L-amino acid transmembrane transporter activity
TFRC	**Transferrin receptor protein 1**	Plasma membrane	Cellular uptake of iron
ITGB1	**Integrin beta-1**	Plasma membrane	Cell adhesion, regulates cytokinesis
LDHB	**L-lactate dehydrogenase B chain**	Cytoplasm	Belongs to the LDH/MDH superfamily.
PTK7	**Inactive tyrosine-protein kinase 7**	Plasma membrane	Cell adhesion, cell migration, cell polarity, proliferation, actin cytoskeleton reorganization and apoptosis.
DSG2	**Desmoglein-2**	Plasma membrane	Interaction of plaque proteins and intermediate filaments mediating cell-cell adhesion.
PTPRF	**Receptor-type tyrosine-protein phosphatase F**	Plasma membrane	Cell adhesion receptor

CDH2	**Cadherin-2**	Plasma membrane	N-cadherin
CADM1	**Cell adhesion molecule 1**	Plasma membrane	Cell adhesion
CD276	**CD276 antigen**	Plasma membrane	Regulation of T-cell mediated immune response
DAG1	**Dystroglycan**	Plasma membrane	Provides a link between laminin in the extracellular matrix and dystrophin in the membrane cytoskeleton.
ITGA2	**Integrin alpha-1**	Plasma membrane	Cell adhesion, force generation, and organization of newly synthesized extracellular matrix.
PPP2R2D	**Serine/threonine-protein phosphatase 2A 55 kDa regulatory subunit B delta isoform**	Cytosol	Control of mitosis entry and exit
GCN1	**eIF-2-alpha kinase activator GCN1**	Cytosol	Cellular response to amino acid starvation
LDHA	**L-lactate dehydrogenase A chain**	Cytosol	Belongs to the LDH family.
ATP1A1	**Sodium/potassium-transporting ATPase subunit alpha-1**	Plasma membrane	ATPase coupled cation transmembrane transporter activity
PGK1	**Phosphoglycerate kinase 1**	Cytosol	Glycolysis

CXADR	**Coxsackievirus and adenovirus receptor**	Plasma membrane	Cell adhesion
ADGRL2	**Adhesion G protein-coupled receptor L2**	Plasma membrane	Regulation of exocytosis
ROBO1	**Roundabout homolog 1**	Plasma membrane	Regulation of cell migration, inhibition MYO9B-mediated stimulation of RHOA-GTPase activity.
EPHA2	**Ephrin type-A receptor 2**	Plasma membrane	Cell migration, integrin-mediated adhesion, proliferation and differentiation of cells.
HNRNPA3	**Heterogeneous nuclear ribonucleoprotein A3**	Nucleus	Cytoplasmic trafficking of RNA.
ATP1B3	**Sodium/potassium-transporting ATPase subunit beta-3**	Plasma membrane	ATPase coupled cation transmembrane transporter activity
ATP1B1	**Sodium/potassium-transporting ATPase subunit beta-1**	Plasma membrane	ATPase coupled cation transmembrane transporter activity
CAPZA2	**F-actin-capping protein subunit alpha-2**	Cortical Actin Cytoskeleton	F-actin-capping proteins bind in a Ca(2+)-independent manner to the fast growing ends of actin filaments.
NCAM1	**Neural cell adhesion molecule 1**	Plasma membrane	Neuron-neuron adhesion

PFKL	**ATP-dependent 6-phosphofructokinase, liver type**	Cytosol	Glycolysis
PDE12	**2',5'-phosphodiesterase 12**	Cytosol	Negative regulator of the The 2-5A system
F11R	**Junctional adhesion molecule A**	Plasma membrane	Epithelial tight junction formation
FLNA	**Filamin-A**	Actin cytoskeleton	Promotes orthogonal branching of actin filaments and links actin filaments to membrane glycoproteins. Anchors various transmembrane proteins to the actin cytoskeleton and serves as a scaffold for a wide range of cytoplasmic signaling proteins.
GSTP1	**Glutathione S-transferase P**	Nucleus, Mitochondrion	Negative regulation of CDK5 activity via p25/p35 translocation.
XPO1	**Exportin-1**	Nucleus	Nuclear export of cellular proteins and RNAs.
CLTC	**Clathrin heavy chain 1**	Mitotic Spindle	Stabilization of kinetochore fibers of the mitotic spindle, Maintenance of kinetochore fiber tension
PPP2R1A	**Serine/threonine-protein phosphatase 2A 65 kDa regulatory subunit A alpha isoform**	Plasma membrane, Nucleus	Required for proper chromosome segregation and for centromeric localization of SGO1 in mitosis.
HNRNPD	**Heterogeneous nuclear ribonucleoprotein D0**	Nucleus	RNA binding
HSP90B1	**Endoplasmin**	ER, Plasma membrane	Processing and transport of secreted proteins.

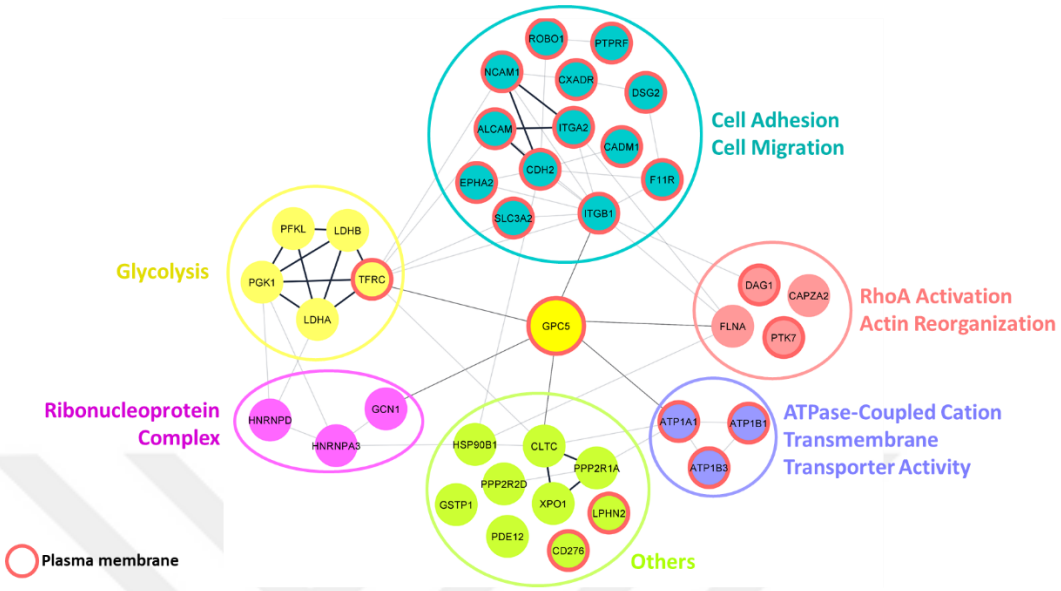

Figure 4. 23: Network clustering of interaction partners of GPC5 during cytokinesis

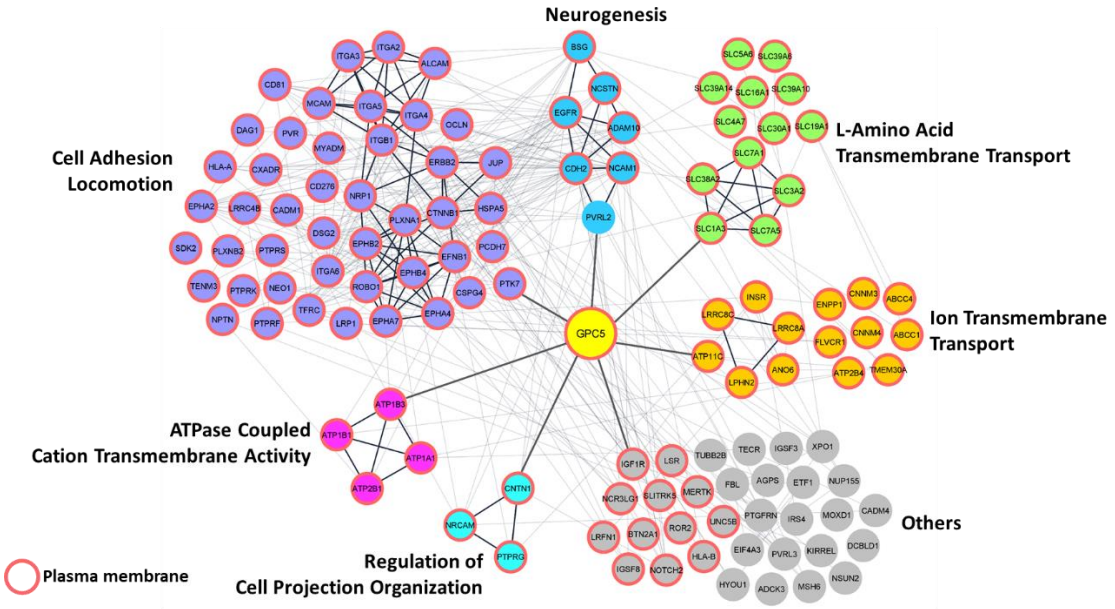

Figure 4. 24: Network clustering of interaction partners of GPC5 at interphase.

After identifying the interaction partners of GPC5 at interphase and cytokinesis, we compared the relative strength of interactions between GPC5 and its interactors. For this purpose, we compared relative PSM values of common interactors which are normalized by average PSM value to eliminate differences in detection rates of each experiment and to bring all samples to the same scale. This analysis revealed that the strength of interaction of common interactors were decreased during cytokinesis compared to interphase. Log Fold Change values of the analysis are listed in *Table 4.4*.

Table 4. 4: Relative strength of interaction between GPC5 and the common interactors during interphase and cytokinesis

Gene Name	LogFoldChange
PTPRF	-2.80980041
ITGA2	-2.266751689
ATP1B3	-2.264451735
DSG2	-1.998505813
CDH2	-1.908780061
CXADR	-1.882977988
ADGRL2	-1.877857262
TFRC	-1.861464071
PTK7	-1.671364895
ROBO1	-1.350202002
EPHA2	-1.201248835
CD276	-1.153344532
ATP1A1	-1.070898898
NCAM1	-1.038278028
ATP1B1	-0.924805224
SLC3A2	-0.805302762
ITGB1	-0.766393846
DAG1	-0.761404405
CADM1	-0.680227485
ALCAM	-0.638251155
GPC5	-0.427332745

4.3.3 Interaction Partners of GPC3 During Cytokinesis

We identified 635 significant proteins in interphase cells as GPC3 interactors by SAINT analysis. This very high number is due to the lack of enough biological replicates. In HEK293T cells synchronized to monopolar cytokinesis, 22 proteins were identified as GPC3 interactors and all of them are common in interphase and cytokinesis cells as illustrated in the Venn diagram in **Figure 4.24**.

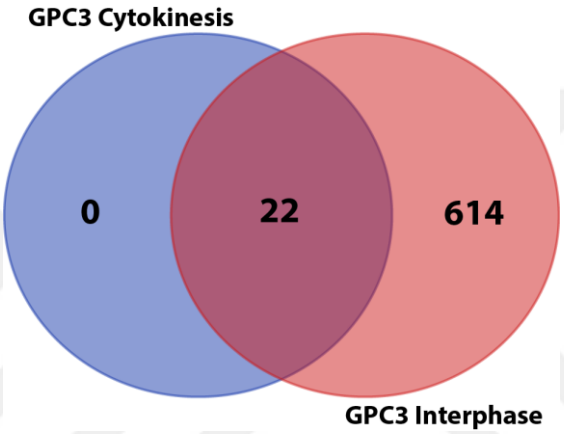

Figure 4. 25: Venn diagram showing the common GPC3 interactors in interphase and in cytokinesis of HEK293T cells.

Cellular localizations and functions of interaction partners of GPC3 during cytokinesis is listed in *Table 4.5*. Localizations and molecular functions of these proteins have been retrieved from UniProt database. Network clustering of GPC3 interactors during cytokinesis is illustrated in **Figure 4.25**. Additionally, common interaction partners of GPC3 and GPC5 during cytokinesis is highlighted in **Figure 4.26**.

,

Table 4. 5: Cellular localizations and functions of interaction partners of GPC3 during cytokinesis.

Gene Name	Protein Name	Cellular Localization	Function
ATP1A1	**Sodium/potassium-transporting ATPase subunit alpha-1**	Plasma membrane	ATPase coupled cation transmembrane transporter activity
HSPA5	**Endoplasmic reticulum chaperone BiP**	ER	Protein folding and quality control
ALCAM	**CD166 antigen**	Plasma membrane	Cell adhesion
TFRC	**Transferrin receptor protein 1**	Plasma membrane	Cellular uptake of iron
SLC16A1	**Monocarboxylate transporter 1**	Plasma membrane	Rapid transport across the plasma membrane of monocarboxylates
BSG	**Basigin**	Plasma membrane	Cell-cell adhesion mediator
SLC3A2	**4F2 cell-surface antigen heavy chain**	Plasma membrane	Aromatic amino acid transmembrane transporter activity
ITGA2	**Integrin alpha-2**	Plasma membrane	Cell adhesion, force generation, and organization of newly synthesized extracellular matrix.
CDH2	**Cadherin-2**	Plasma membrane	N-cadherin
ITGB1	**Integrin beta-1**	Plasma membrane	Cell adhesion, regulates cytokinesis
ATP1B3	**Sodium/potassium-transporting ATPase subunit beta-3**	Plasma membrane	ATPase coupled cation transmembrane transporter activity
NOTCH2	**Neurogenic locus notch homolog protein 2**	Plasma membrane	Signaling receptor

PRDX4	**Peroxiredoxin-4**	ER	Cell protection against oxidative stress
PTK7	**Inactive tyrosine-protein kinase 7**	Plasma membrane	Cell adhesion, cell migration, cell polarity, proliferation, actin cytoskeleton reorganization and apoptosis.
NPTN	**Neuroplastin**	Plasma membrane	Cell adhesion molecule
CD276	**CD276 antigen**	Plasma membrane	Regulation of T-cell mediated immune response
EPHA2	**Ephrin type-A receptor 2**	Plasma membrane	Regulates cell adhesion and differentiation through DSG1 and inhibition of the ERK1/ERK2 signaling pathway.
LRRC8A	**Volume-regulated anion channel subunit LRRC8A**	Plasma membrane	Volume-sensitive anion channel activity
LSR	**Lipolysis-stimulated lipoprotein receptor**	Plasma membrane	Tricellular tight junction assembly
PLXNB2	**Plexin-B2**	Plasma membrane	RHOA activation and subsequent changes of the actin cytoskeleton.
ATP1B1	**Sodium/potassium-transporting ATPase subunit beta-1**	Plasma membrane	ATPase coupled cation transmembrane transporter activity

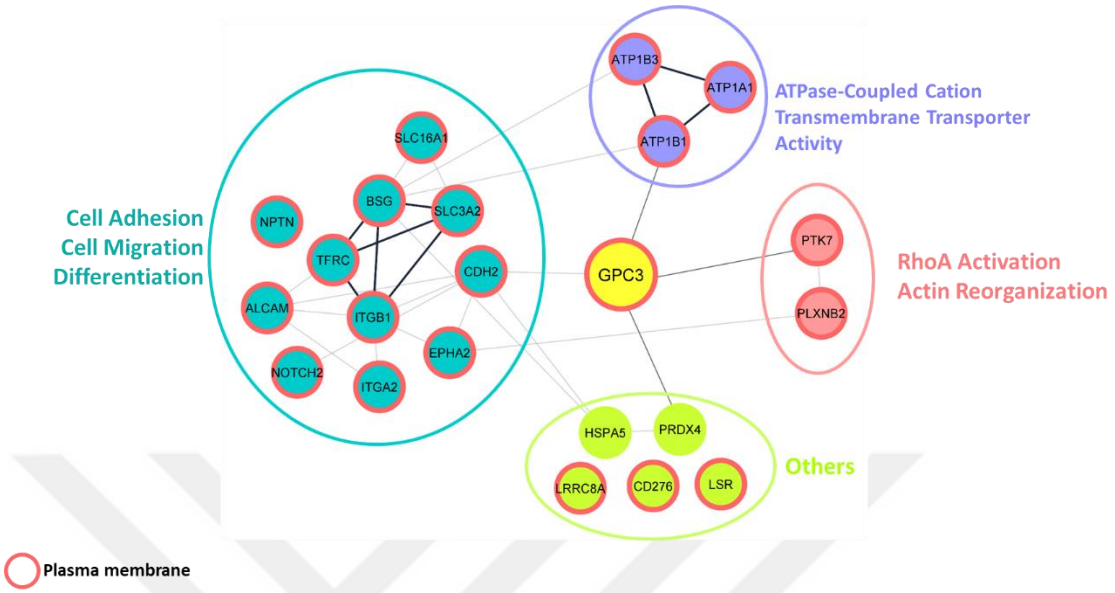

Figure 4. 26: Network clustering of interaction partners of GPC3 during cytokinesis.

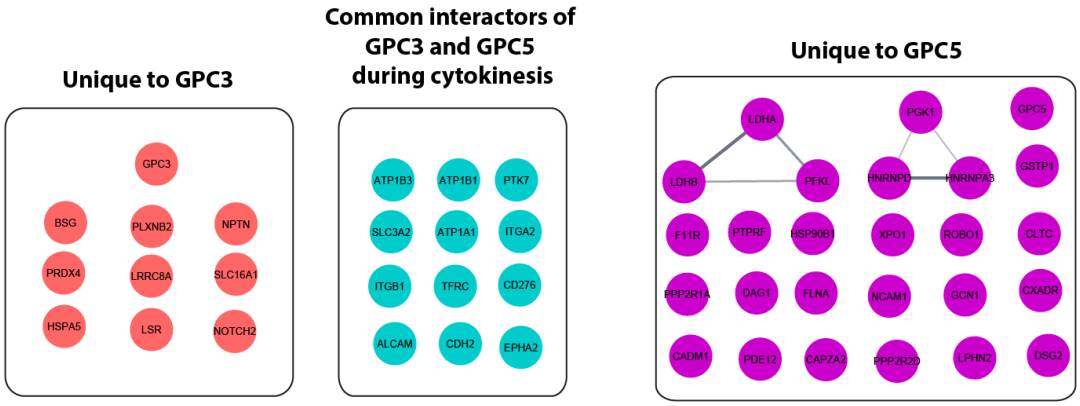

Figure 4. 27: Common Interaction Partners of GPC3 and GPC5 during cytokinesis

Chapter 5:

DISCUSSION

In this study, we aimed to identify the roles of Glypicans 3 and 5 during cytokinesis. We first examined the localization dynamics of Glypicans 3 and 5 during cell division. To observe localization dynamics of GPC3 and GPC5 during mitosis, we transfected HeLa Kyoto cells with EGFP-tagged GPC3 and GPC5 constructs separately and performed live cell fluorescent imaging analyses. As, controls we transfected HeLa Kyoto cells with myr-PALM-GFP construct. During mitosis, both GPC3 and GPC5 localized to the plasma membrane. For cleavage furrow enrichment analysis, we measured the average GFP intensities at the cleavage furrow in mid telophase cells. For normalization, we divided these values to the average pole intensities of each cell. Statistical analysis comparing the normalized GFP intensities of GPC3 and GPC5 to those of myr-PALM-GFP at mid telophase revealed that both GPC3 and GPC5 significantly enriches at the cleavage furrow during cytokinesis.

After showing that both GPC3 and GPC5 enrich at the cleavage furrow during cytokinesis, we investigated the division phenotypes of GPC5 knockout cells. For this purpose, we first recapitulate Eggert Group's findings that siRNA mediated knock-down of GPC5 lead to binucleation in HeLa and HCE cells (Data not published). To recapitulate these results, we created inducible GPC5 knockout HeLa cells. These cells stably express GPC5 sgRNAs (designed by Dr. Federico Dona, Eggert Group, King's College London) and only express Cas9 protein upon 72-hour Doxycycline induction. In both HeLaCas9 GPC5 sg1.8 cells (Dox inducible GPC5 knockout cell line created by Dr. Federico Dona, Eggert Group, King's College London) and HeLaCas9 GPC5 sg2 cells, upon induction of GPC5 knockout, we observed a significant increase in the multinucleated cells compared to controls. Furthermore, this multinucleation phenotype could be rescued using CRISPR-resistant cMyc-GPC5 construct (Created by Dr. Federico Dona, Eggert

Group, King's College London). These results further supported the idea that GPC5 has important roles during cytokinesis.

After we showed that GPC5 knockout leads to multinucleation, we wanted to check the cellular localizations of known cytokinesis proteins in GPC5 knockout cells. Because many studies have shown that Phospho-myosin, Ezrin, p-ERM, Anillin and Alix are necessary for a successful cytokinesis [2, 12, 13, 57], we performed immunostaining in GPC5 knockout and control samples for these proteins and checked their localizations in dividing cells. The preliminary experiments showed no significant effect of GPC5 knockout on the localizations of the above-mentioned proteins. Time dependent analyses with better resolution is required to make further comments.

To further investigate the possible roles of GPC5 during cytokinesis, we analyzed the division phenotypes of GPC5 knockout cells using live cell fluorescent and bright field imaging analyses. In our live cell imaging analyses, we observed that GPC5 knockout causes defects at different stages of cell division. First, we identified chromosome jiggling phenotype in GPC5 knockout cells. In 11.43% of the dividing GPC5 knockout cells, chromosomes were moving from one pole to the other for a long time before they were finally stabilized and formed the metaphase plate whereas only 1.79% of the control cells showed a similar phenotype. However, these increase in the chromosome jiggling phenotype was not statistically significant. Unlike chromosome jiggling phenotype, we showed that GPC5 knockout cells exhibit significant defects in division plane orientation as well as significantly increased cleave furrow and polar blebbing and significantly delay in midbody abscission. These significant increases in cleavage furrow and polar blebbing phenotypes might indicate a cortical actin instability [58].

HRP-based proximity labelling experiments revealed both Glypicans 3 and 5 might interact with proteins that are involved in cell adhesion, ATPase-coupled cation transmembrane transport, and RhoA activation and actin cytoskeleton reorganization. Among those, the relationships between ITGB1 and PTK7 can be further investigated since previous studies showed their involvement in cytokinesis and RhoA activation [59, 60]. Although our analysis showed that the relative strength of interactions of common

GPC5 interactors is unexpectedly decreased in cytokinesis compared to interphase, biologically this might just imply the decrease in abundance of these proteins during cytokinesis.

Overall, this study showed that Glypicans 3 and 5 enriches at the cleavage furrow during cytokinesis and knockout of *GPC5* leads to defects in cell division and cytokinesis failure. Further molecular investigations of downstream effects of the interactions of Glypicans 3 and 5 with the proteins identified as interaction partners in this study might provide more insights in about their roles is cell division especially in terms of regulation of cortical actin stability.

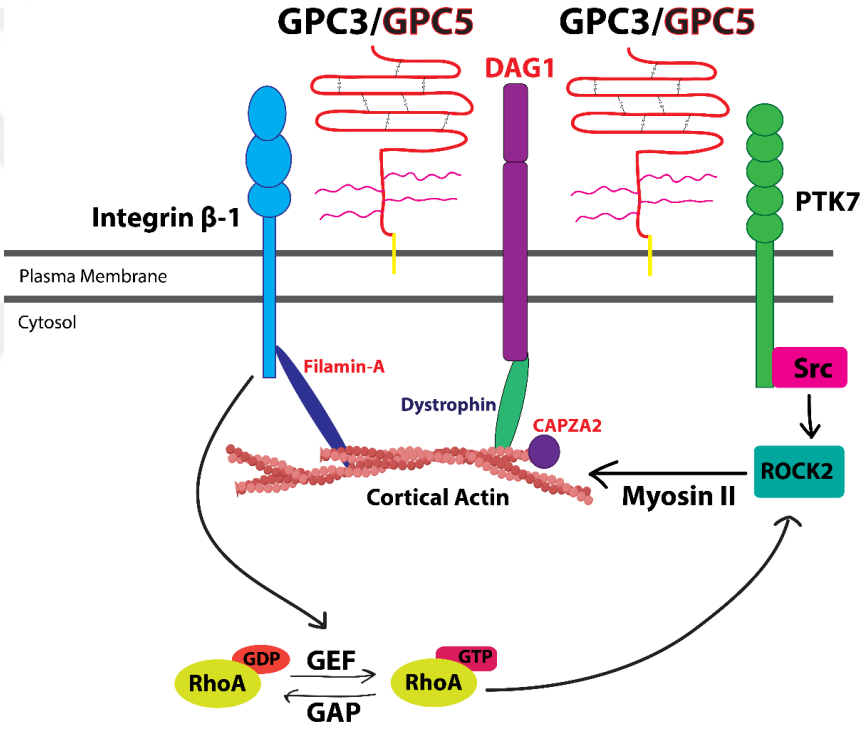

Figure 5. 1: A proposed model of how GPC3 and GPC5 might involve in mammalian cytokinesis.

We propose that GPC3 and GPC5 might be involved in cortical actin stability and regulation of RhoA activation through their interaction partners.

BIBLIOGRAPHY

1. Barr, F.A. and U. Gruneberg, *Cytokinesis: placing and making the final cut.* Cell, 2007. **131**(5): p. 847-60.
2. Green, R.A., E. Paluch, and K. Oegema, *Cytokinesis in animal cells.* Annu Rev Cell Dev Biol, 2012. **28**: p. 29-58.
3. Filmus, J. and M. Capurro, *The role of glypican-3 in the regulation of body size and cancer.* Cell Cycle, 2008. **7**(18): p. 2787-90.
4. Kaur, S.P. and B.S. Cummings, *Role of glypicans in regulation of the tumor microenvironment and cancer progression.* Biochem Pharmacol, 2019. **168**: p. 108-118.
5. Dong, Z., et al., *Down-regulating glypican-3 expression: molecular-targeted therapy for hepatocellular carcinoma.* Mini Rev Med Chem, 2014. **14**(14): p. 1183-93.
6. Schafer, K.A., *The cell cycle: a review.* Vet Pathol, 1998. **35**(6): p. 461-78.
7. Vermeulen, K., D.R. Van Bockstaele, and Z.N. Berneman, *The cell cycle: a review of regulation, deregulation and therapeutic targets in cancer.* Cell Prolif, 2003. **36**(3): p. 131-49.
8. Civelekoglu-Scholey, G. and D. Cimini, *Modelling chromosome dynamics in mitosis: a historical perspective on models of metaphase and anaphase in eukaryotic cells.* Interface Focus, 2014. **4**(3): p. 20130073.
9. Barnum, K.J. and M.J. O'Connell, *Cell cycle regulation by checkpoints.* Methods Mol Biol, 2014. **1170**: p. 29-40.
10. Otto, T. and P. Sicinski, *Cell cycle proteins as promising targets in cancer therapy.* Nat Rev Cancer, 2017. **17**(2): p. 93-115.
11. Peters, J.M., *The anaphase promoting complex/cyclosome: a machine designed to destroy.* Nat Rev Mol Cell Biol, 2006. **7**(9): p. 644-56.
12. Fededa, J.P. and D.W. Gerlich, *Molecular control of animal cell cytokinesis.* Nat Cell Biol, 2012. **14**(5): p. 440-7.
13. Normand, G. and R.W. King, *Understanding cytokinesis failure.* Adv Exp Med Biol, 2010. **676**: p. 27-55.
14. Schroeder, T.E., *The contractile ring. II. Determining its brief existence, volumetric changes, and vital role in cleaving Arbacia eggs.* J Cell Biol, 1972. **53**(2): p. 419-34.
15. Caballe, A. and J. Martin-Serrano, *ESCRT machinery and cytokinesis: the road to daughter cell separation.* Traffic, 2011. **12**(10): p. 1318-26.
16. Li, N., et al., *Glypicans as Cancer Therapeutic Targets.* Trends Cancer, 2018. **4**(11): p. 741-754.
17. Li, N., M.R. Spetz, and M. Ho, *The Role of Glypicans in Cancer Progression and Therapy.* J Histochem Cytochem, 2020. **68**(12): p. 841-862.
18. Song, H.H. and J. Filmus, *The role of glypicans in mammalian development.* Biochim Biophys Acta, 2002. **1573**(3): p. 241-6.
19. Filmus, J. and M. Capurro, *The role of glypicans in Hedgehog signaling.* Matrix Biol, 2014. **35**: p. 248-52.
20. Fico, A., F. Maina, and R. Dono, *Fine-tuning of cell signaling by glypicans.* Cell Mol Life Sci, 2011. **68**(6): p. 923-9.
21. Traister, A., W. Shi, and J. Filmus, *Mammalian Notum induces the release of glypicans and other GPI-anchored proteins from the cell surface.* Biochem J, 2008. **410**(3): p. 503-11.

22. Capurro, M., et al., *Processing by convertases is required for glypican-3-induced inhibition of Hedgehog signaling.* J Biol Chem, 2015. **290**(12): p. 7576-85.
23. Nishida, T. and H. Kataoka, *Glypican 3-Targeted Therapy in Hepatocellular Carcinoma.* Cancers (Basel), 2019. **11**(9).
24. Wu, Y., T.Y. Belenkaya, and X. Lin, *Dual roles of Drosophila glypican Dally-like in Wingless/Wnt signaling and distribution.* Methods Enzymol, 2010. **480**: p. 33-50.
25. Veugelers, M., et al., *Characterization of glypican-5 and chromosomal localization of human GPC5, a new member of the glypican gene family.* Genomics, 1997. **40**(1): p. 24-30.
26. Saunders, S., S. Paine-Saunders, and A.D. Lander, *Expression of the cell surface proteoglycan glypican-5 is developmentally regulated in kidney, limb, and brain.* Dev Biol, 1997. **190**(1): p. 78-93.
27. Williamson, D., et al., *Role for amplification and expression of glypican-5 in rhabdomyosarcoma.* Cancer Res, 2007. **67**(1): p. 57-65.
28. Nishimura, R., et al., *Characterization of genetic lesions in rhabdomyosarcoma using a high-density single nucleotide polymorphism array.* Cancer Sci, 2013. **104**(7): p. 856-64.
29. Zhang, Y., et al., *The role of GPC5 in lung metastasis of salivary adenoid cystic carcinoma.* Arch Oral Biol, 2014. **59**(11): p. 1172-82.
30. Li, Y., et al., *Genetic variants and risk of lung cancer in never smokers: a genome-wide association study.* Lancet Oncol, 2010. **11**(4): p. 321-30.
31. Yang, X., et al., *Glypican-5 is a novel metastasis suppressor gene in non-small cell lung cancer.* Cancer Lett, 2013. **341**(2): p. 265-73.
32. Yuan, S., et al., *GPC5, a novel epigenetically silenced tumor suppressor, inhibits tumor growth by suppressing Wnt/beta-catenin signaling in lung adenocarcinoma.* Oncogene, 2016. **35**(47): p. 6120-6131.
33. Li, Y., et al., *The overexpression of glypican-5 promotes cancer cell migration and is associated with shorter overall survival in non-small cell lung cancer.* Oncol Lett, 2013. **6**(6): p. 1565-1572.
34. Zhang, C., et al., *A lung cancer gene GPC5 could also be crucial in breast cancer.* Mol Genet Metab, 2011. **103**(1): p. 104-5.
35. Zhang, C., et al., *Prognostic significance of GPC5 expression in patients with prostate cancer.* Tumour Biol, 2016. **37**(5): p. 6413-8.
36. Yuan, Q., et al., *High expression of microRNA-4295 contributes to cell proliferation and invasion of pancreatic ductal adenocarcinoma by the down-regulation of Glypican-5.* Biochem Biophys Res Commun, 2018. **497**(1): p. 73-79.
37. Liu, T., et al., *miR-709 up-regulated in hepatocellular carcinoma, promotes proliferation and invasion by targeting GPC5.* Cell Prolif, 2015. **48**(3): p. 330-7.
38. Hong, X., et al., *MicroRNA-301b promotes the proliferation and invasion of glioma cells through enhancing activation of Wnt/β-catenin signaling via targeting Glypican-5.* Eur J Pharmacol, 2019. **854**: p. 39-47.
39. Li, F., et al., *Glypican-5 stimulates rhabdomyosarcoma cell proliferation by activating Hedgehog signaling.* J Cell Biol, 2011. **192**(4): p. 691-704.
40. Yuan, S., et al., *GPC5, a novel epigenetically silenced tumor suppressor, inhibits tumor growth by suppressing Wnt/β-catenin signaling in lung adenocarcinoma.* Oncogene, 2016. **35**(47): p. 6120-6131.

41. Ho, M., *Advances in liver cancer antibody therapies: a focus on glypican-3 and mesothelin.* BioDrugs, 2011. **25**(5): p. 275-84.
42. Li, N., et al., *A Frizzled-Like Cysteine-Rich Domain in Glypican-3 Mediates Wnt Binding and Regulates Hepatocellular Carcinoma Tumor Growth in Mice.* Hepatology, 2019. **70**(4): p. 1231-1245.
43. Gao, W., H. Kim, and M. Ho, *Human Monoclonal Antibody Targeting the Heparan Sulfate Chains of Glypican-3 Inhibits HGF-Mediated Migration and Motility of Hepatocellular Carcinoma Cells.* PLoS One, 2015. **10**(9): p. e0137664.
44. Aviel-Ronen, S., et al., *Glypican-3 is overexpressed in lung squamous cell carcinoma, but not in adenocarcinoma.* Mod Pathol, 2008. **21**(7): p. 817-25.
45. Nakatsura, T., et al., *Identification of glypican-3 as a novel tumor marker for melanoma.* Clin Cancer Res, 2004. **10**(19): p. 6612-21.
46. Maeda, D., et al., *Glypican-3 expression in clear cell adenocarcinoma of the ovary.* Mod Pathol, 2009. **22**(6): p. 824-32.
47. Yamanaka, K., et al., *Immunohistochemical study of glypican 3 in thyroid cancer.* Oncology, 2007. **73**(5-6): p. 389-94.
48. Pilia, G., et al., *Mutations in GPC3, a glypican gene, cause the Simpson-Golabi-Behmel overgrowth syndrome.* Nat Genet, 1996. **12**(3): p. 241-7.
49. Xiang, Y.Y., V. Ladeda, and J. Filmus, *Glypican-3 expression is silenced in human breast cancer.* Oncogene, 2001. **20**(50): p. 7408-12.
50. Murthy, S.S., et al., *Expression of GPC3, an X-linked recessive overgrowth gene, is silenced in malignant mesothelioma.* Oncogene, 2000. **19**(3): p. 410-6.
51. Valsechi, M.C., et al., *GPC3 reduces cell proliferation in renal carcinoma cell lines.* BMC Cancer, 2014. **14**: p. 631.
52. Guo, M., et al., *Glypican-3: A New Target for Diagnosis and Treatment of Hepatocellular Carcinoma.* J Cancer, 2020. **11**(8): p. 2008-2021.
53. Fleming, B.D. and M. Ho, *Development of Glypican-3 Targeting Immunotoxins for the Treatment of Liver Cancer: An Update.* Biomolecules, 2020. **10**(6).
54. Shimizu, Y., et al., *Next-Generation Cancer Immunotherapy Targeting Glypican-3.* Front Oncol, 2019. **9**: p. 248.
55. Capurro, M.I., et al., *Glypican-3 inhibits Hedgehog signaling during development by competing with patched for Hedgehog binding.* Dev Cell, 2008. **14**(5): p. 700-11.
56. Capurro, M.I., F. Li, and J. Filmus, *Overgrowth of a mouse model of Simpson-Golabi-Behmel syndrome is partly mediated by Indian hedgehog.* EMBO Rep, 2009. **10**(8): p. 901-7.
57. Wu, Q., et al., *Deficiency in myosin light-chain phosphorylation causes cytokinesis failure and multipolarity in cancer cells.* Oncogene, 2010. **29**(29): p. 4183-93.
58. Charras, G.T., et al., *Reassembly of contractile actin cortex in cell blebs.* J Cell Biol, 2006. **175**(3): p. 477-90.
59. Pellinen, T., et al., *Integrin trafficking regulated by Rab21 is necessary for cytokinesis.* Dev Cell, 2008. **15**(3): p. 371-85.
60. Sebbagh, M. and J.P. Borg, *Insight into planar cell polarity.* Exp Cell Res, 2014. **328**(2): p. 284-95.

VITA

Ezgi Memiş was born in İstanbul, Turkey. She graduated from from Aydın Adnan Menderes Anatolian High School in 2012 and then received her B.Sc. degree in Molecular Biology and Genetics from Boğaziçi University, İstanbul, Turkey in 2018. From September 2018 to January 2021, she worked as a research and teaching assistant at Koç University, İstanbul, Turkey where she also studied her M.Sc. research on “Roles of Cell Surface Proteins During Cytokinesis”.